Assessing the Impact of Climate Change on Agricultural Water Consumption Using Remote Sensing Data and Machine Learning: A Case Study of Zankalon, Nile Delta, Egypt

Ahmed Sakna[1,*], Bich Ngoc Tran[2,3], Solomon Seyoum[2], Marloes Mul[2], Muhammad Rasool Al-Kilani[4]

[1]UNESCO Regional Office for Egypt and Sudan, Cairo, Egypt.

[2]Land and Water Management, IHE Delft Institute for Water Education, Delft, the Netherlands.

[3]Water Management, Delft University of Technology, Delft, the Netherlands.

[4]Department of Land, Water and Environment, School of Agriculture, The University of Jordan, Amman, 11942, Jordan.

*Corresponding author: ahmadsakna96@gmail.com

Abstract

The Nile Delta, one of Egypt's key agricultural hubs, is becoming increasingly affected by climate change, impacting its water resources and agricultural productivity. Although previous studies have examined broad-scale climate impacts on agriculture in the region, crop-specific projections of agricultural water consumption at the field scale remain scarce, particularly for the Nile Delta. This study aims to quantify the effects of projected climate change on agricultural water consumption in Zankalon, Nile Delta, Egypt, using a combination of machine learning (ML) and satellite remote sensing.

Crop-specific Actual Evapotranspiration and Interception (AETI) at 30 m resolution was derived from the FAO WaPOR v2 portal (2009–2023). Dekadal meteorological variables from the AgERA5 reanalysis and an ensemble of 23 CMIP6 General Circulation Models served as predictor variables for ML models trained for six major crops. After evaluating nine ML algorithm types, the best-performing algorithm per crop was selected for projection (Random

Forest for orchards and wheat; SVR for rice, grapes, and potato; Ridge for clover), with test-set R^2 values ranging from 0.68 to 0.86, under two Shared Socioeconomic Pathways (SSPs): SSP2-4.5, which stabilises radiative forcing at 4.5 W m^{-2} by 2100, and SSP5-8.5, which stabilises at 8.5 W m^{-2} by 2100 — extending projections to 2099.

Temperature and solar radiation are the primary AETI drivers in Zankalon, with seasonal cropping patterns exerting a strong modulating effect. The results reveal a counter-intuitive seasonal pattern: winter crops (wheat, clover) show *increasing* growing-season water consumption (+5.3–6.6% by 2099 under SSP5-8.5), driven by projected warming of the cool growing season, while summer crops (rice, grapes) show *decreasing* AETI (-4.7% to -6.3%), likely reflecting projected changes in summer humidity and radiation balance. Specifically, orchards reach $+4.2\,\%$ and potato shows near-neutral change ($\approx+0.4\,\%$) by 2099 under SSP5-8.5, while rice declines by up to $-6.3\,\%$ under SSP2-4.5 and grapes by up to $-4.0\,\%$ under SSP2-4.5. Incorporating planned agricultural expansion raises total Crop Water Requirements (CWR) by 13.5 % by 2050—substantially exceeding the 3.6 % increase attributable to climate change alone. These findings highlight the necessity of crop-specific, adaptive water management strategies for the Nile Delta. The projected increases in winter-crop water demand, combined with planned national expansion, underscore the importance of soil-moisture-based precision irrigation [Abdelal et al., 2026] and high-efficiency field practices as critical tools for managing future water scarcity.

Keywords: Climate Change; Agricultural Water Consumption; AETI; Remote Sensing; Machine Learning; Nile Delta; WaPOR; CMIP6; SSP Scenarios

1 Introduction

The Nile Delta, defined by its intensive agriculture and one of the world's highest population densities, faces the compounding pressures of severe water scarcity and accelerating climate change [Roushdi, 2024]. Egypt's society and economy are fundamentally dependent on the Nile River, which supplies nearly 79 % of water to an agricultural sector that consumes over 80 % of the country's total freshwater resources [IDSC, 2021, Satoh et al., 2017]. This extreme dependence on a single source, combined with limited and over-exploited groundwater aquifers, creates deep structural water vulnerability [Hamed et al., 2022, Esraa et al., 2023, Masoud, 2020]. The country already faces an estimated annual water deficit of 13.5 billion cubic metres [Omar et al., 2021], exacerbated by the widespread use of traditional, low-efficiency surface irrigation [Ayyad et al., 2019]. Simultaneously, the agricultural sector must expand production to ensure food security for a rapidly growing population — placing national development goals in direct conflict with water availability [El-Ramady et al., 2013, Elsharkawy et al., 2022].

Climate change is amplifying this crisis through specific, measurable shifts in the Nile Delta's climate. Observed and projected trends include rising mean and maximum temperatures, increasing reference evapotranspiration, and more erratic precipitation [Hamed et al., 2022, Elbeltagi et al., 2020, Shalby et al., 2020]. Critically, climate projections indicate that temperature seasonality will intensify: hotter summers will drive greater atmospheric evaporative demand, while relatively milder winters may reduce cold-season crop water requirements [Intergovernmental Panel on Climate, 2023]. These changes translate into higher crop water requirements for summer crops and altered growing conditions for winter crops. Recent work by Sobh et al. [2025] confirmed that reference evapotranspiration over Egypt is projected to increase under all CMIP6 SSP scenarios through to 2100, with the greatest increases occurring in winter, providing direct physical context for the seasonal AETI responses investigated here.

Understanding these crop-specific, seasonal responses is essential for water resources planning in the Nile Delta, yet reliable, high-resolution projections remain scarce. To address this, researchers increasingly combine satellite remote sensing and climate modelling. Satellite-derived AETI products, such as those from the FAO WaPOR portal [Food and Agriculture Organization of the United Nations, 2019], provide high-resolution diagnostic data on current

crop water consumption but lack predictive capability. Recent evaluations have confirmed WaPOR as a reliable product in arid irrigated systems, with correlations to ground-measured ET of 0.69–0.88 [Chirimab et al., 2025], and demonstrated its utility for agricultural water accounting across water-scarce basins [Al-Omoush et al., 2025]. Global Climate Models (GCMs) from the Coupled Model Intercomparison Project Phase 6 (CMIP6) [Eyring et al., 2016] project plausible futures under different Shared Socioeconomic Pathways, but their coarse spatial resolution ($\sim$100 km) cannot resolve the fine-scale heterogeneity of irrigated agricultural landscapes. This scale mismatch between local needs and coarse global projections represents the central methodological challenge motivating this study [Payus et al., 2020, Zhang et al., 2022].

Previous research and remaining gap

Several studies have examined climate change impacts on evapotranspiration and crop water requirements in Egypt and the broader Nile Basin. Roushdi [2024] projected CWR increases for winter crops in the western Nile Delta using process-based modelling with CMIP5 data. Elbeltagi et al. [2020] demonstrated rising water footprints for wheat and maize under RCP scenarios. M. El-Marsafawy et al. [2018] documented three-decade trends in crop water productivity across the Nile Delta. More recently, Sobh et al. [2025] used four CMIP6 GCMs to project reference ETo increases of up to 14.2 % under SSP5-8.5 by 2100 over Egypt, with the largest increases concentrated in the winter season. Beyond Egypt, Pan et al. [2020] demonstrated the utility of machine learning for estimating global terrestrial evapotranspiration from satellite observations, and Gupta and Kumar [2024] showed that neural networks reproduce reference ET at daily time steps with high accuracy. Several recent studies have demonstrated the use of remote sensing and machine learning to estimate evapotranspiration [Pan et al., 2020, Bochenek and Ustrnul, 2022, Wang, 2023, Al-Sahaf et al., 2025]; however, these approaches have rarely been applied to crop-specific projections in the Nile Delta using high-resolution WaPOR AETI combined with CMIP6 ensemble projections [Elsadek et al., 2023]. Recent progress in ML-based ET projection with CMIP6 in comparable semi-arid settings—including Random Forest and ANN models applied to the Aras River Basin [Ganjei et al., 2026] and explainable ML frameworks for irrigation water productivity [Gao et al., 2026]—demonstrates the growing

maturity of the statistical downscaling approach applied here.

This study addresses this gap by developing an ML-based statistical downscaling framework that: (i) uses 30 m WaPOR AETI as the target variable; (ii) trains models on high-quality AgERA5 reanalysis data; and (iii) applies those trained models to an ensemble median of 23 CMIP6 GCMs to generate crop-specific projections of agricultural water consumption in Zankalon, Nile Delta, under SSP2-4.5 and SSP5-8.5 through 2099. SSP2-4.5 and SSP5-8.5 were selected as they represent an intermediate and a high-end emissions pathway, together spanning the plausible range of future forcing relevant for long-term water resources planning [Intergovernmental Panel on Climate, 2023, Eyring et al., 2016].

Specifically, this study:

(i) identifies the principal climatic drivers of AETI variability for six major crops in Zankalon;

(ii) evaluates all nine ML algorithm types and selects the most robust for future projection; and

(iii) provides crop-specific and seasonally stratified projections of agricultural water consumption and total CWR under climate change and planned expansion scenarios.

Zankalon is a particularly suitable case study because it encompasses the full spectrum of Egypt's major irrigated crops under conditions typical of the eastern Nile Delta, and because high-resolution WaPOR v2 data are available at 30 m for the area, enabling the crop-specific analysis that distinguishes this study from prior work.

2 Methodology

2.1 Study Area

Zankalon (Figure 1) is a rural agricultural community in Egypt's Sharqiyah Governorate, approximately 100 km northeast of Cairo, covering $\sim$1 000 km^2. It is situated within the eastern Nile Delta—a region that supports intensive irrigated agriculture entirely dependent on Nile River water and characteristic of the broader Delta system in terms of crop diversity, irrigation infrastructure, and climate exposure [Food and Agriculture Organization of the United Nations,

2024]. The area has a semi-arid climate with hot, dry summers (25–35 ° C) and mild winters (10–20 ° C), and minimal annual precipitation (<100 mm). All agricultural production is fully dependent on canal irrigation from the Nile River [Intergovernmental Panel on Climate, 2023, World Bank, 2019], making it acutely sensitive to changes in water availability and evaporative demand.

Zankalon was selected for two reasons. First, its cropping system encompasses the six major irrigated crops of the Nile Delta—orchards, wheat, rice, clover, grapes, and potato—across three distinct growing seasons (winter, summer, and nili), making it representative of regional agricultural water use patterns [Osama et al., 2017]. Second, the area is covered by FAO WaPOR v2 Level-3 products at 30 m, providing the high-resolution AETI and Land Cover Classification (LCC) data required for crop-specific analysis. A crop calendar is provided in Table 1 and crop-area distributions are shown in Figure 2.

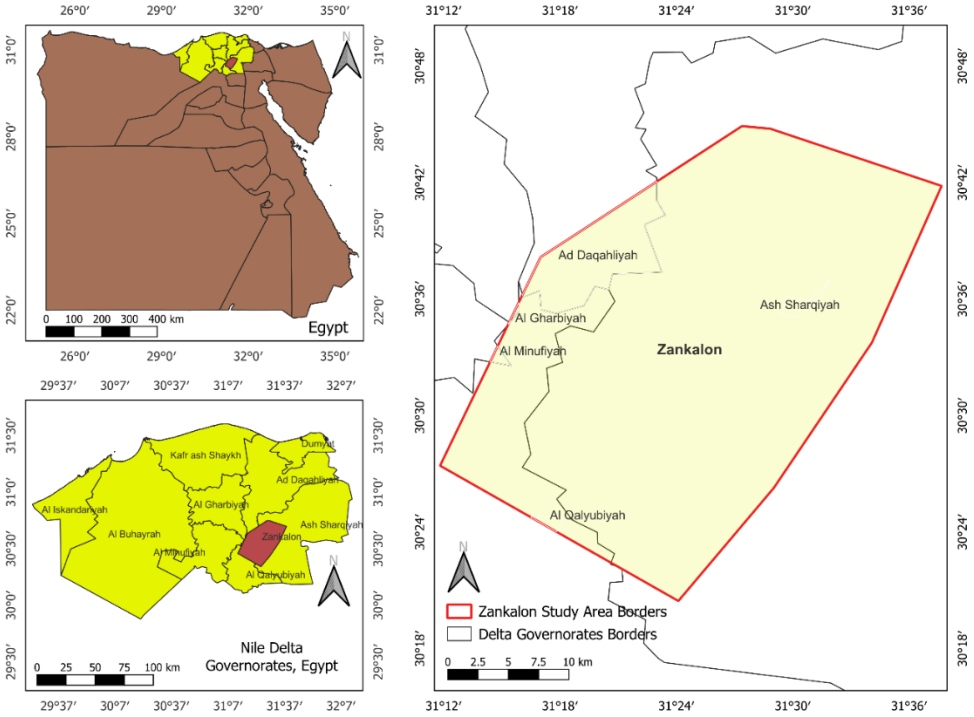

Figure 1: Study area: Zankalon, Nile Delta Governorates, Egypt. The inset shows Zankalon's location within the eastern Nile Delta and the Sharqiyah Governorate.

Table 1: Crop calendar for the six major crops analysed in Zankalon. ✓ = primary growing period; H = typical harvest month(s). Source: adapted from Osama et al. [2017] and Mahmoud and El-Bably [2017].

Crop	Jan	Feb	Mar	Apr	May	Jun	Jul	Aug	Sep	Oct	Nov	Dec
Orchards	✓	✓	✓	✓	✓	✓	✓	✓	✓	✓	✓	✓
Wheat	✓	✓	✓	H							✓	✓
Rice					✓	✓	✓	✓	H			
Clover	✓	✓	H							✓	✓	✓
Grapes			✓	✓	✓	✓	✓	H				
Potato (S1)		✓	✓	✓	H							
Potato (Nili)								✓	✓	✓	H	

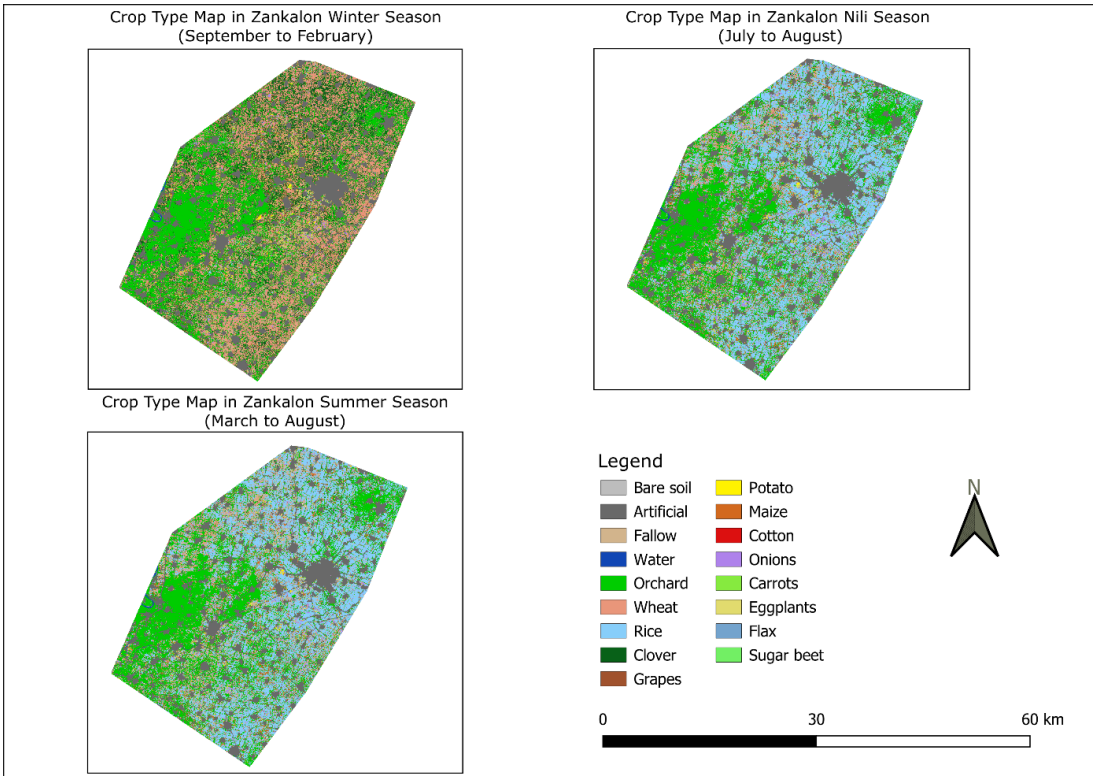

Figure 2: Land use and crop distribution in Zankalon, 2022. Source: Food and Agriculture Organization of the United Nations [2024].

2.2 Methodological Framework

The study followed a four-stage framework (Figure 3): (1) data acquisition; (2) data processing and feature extraction; (3) ML model development and validation; and (4) scenario analysis and

projection.

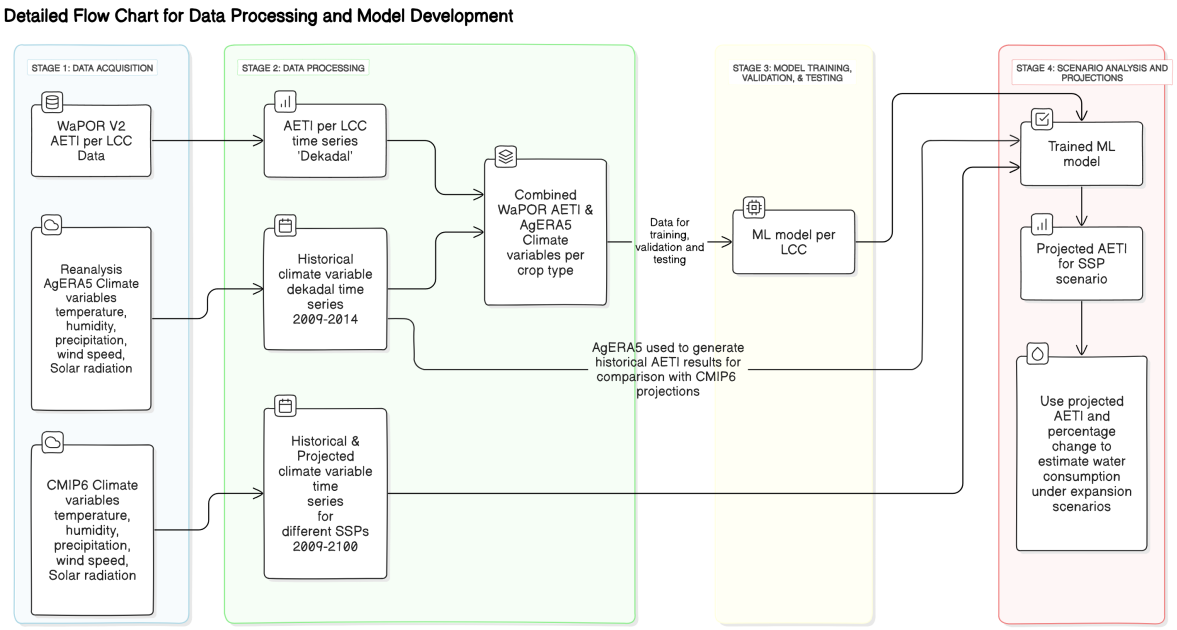

Figure 3: Methodology flowchart. AgERA5 data are used exclusively for ML training and validation; CMIP6 ensemble median data are used only at the projection stage.

2.3 Data Acquisition and Description

A suite of complementary datasets was acquired (Table 2). AgERA5 was selected as the training climate dataset because its spatial resolution (∼9 km) and quality as a reanalysis product constrained by observations are substantially superior to raw CMIP6 output for historical conditions, thereby reducing baseline errors in ML model training [Food and Agriculture Organization of the United Nations, 2020a]. CMIP6 projections were used exclusively to drive the trained models for future periods [Eyring et al., 2016, Zhang et al., 2022].

Table 2: Datasets used in this study. AgERA5 is used for ML training; CMIP6 is used for future projection only.

Type	Dataset	Source	Temporal Res.	Spatial Res.	Period
Satellite	AETI 30 m (WaPOR v2)	FAO CDS	Dekadal	30 m	2009–2023
Satellite	LCC 30 m (WaPOR v2)	FAO CDS	Dekadal	30 m	2009–2023
Reanalysis	AgERA5 (RH, Precip, Solar, Wind, Temp)	Copernicus CDS	Daily→Dekadal	∼9 km	2009–2023
Projection	CMIP6 (23 GCMs; SSP2-4.5 & SSP5-8.5)	Copernicus CDS	Daily→Dekadal	∼100 km	2009–2100

2.3.1 Satellite-Derived AETI and Land Cover Data

High-resolution (30 m) dekadal AETI and LCC were sourced from the FAO WaPOR v2 portal for 2009–2023 [Food and Agriculture Organization of the United Nations, 2019, 2020b]. These data served as the target variable and crop-identification layer for ML model training. Recent independent evaluations have confirmed that WaPOR v2 AETI performs well in arid irrigated settings, with reported RMSE values of 0.87–3.22 mm d^{-1} and correlations of 0.69–0.88 against lysimeter-based observations [Chirimab et al., 2025], providing confidence in its use as a training target variable.

2.3.2 AgERA5 Climate Reanalysis

Daily climate variables (relative humidity, precipitation, solar radiation, wind speed, and temperature: mean, maximum, minimum) at approximately 9 km resolution were acquired from the Copernicus CDS for 2009–2023 [Food and Agriculture Organization of the United Nations, 2020a]. Daily values were aggregated to dekadal resolution by arithmetic averaging (summation for precipitation) to match the WaPOR temporal grid.

2.3.3 CMIP6 Climate Projections

Future climate projections were obtained from an ensemble of 23 CMIP6 GCMs via the Copernicus CDS (https://doi.org/10.24381/cds.c866074c; Eyring et al., 2016). Data were acquired for historical (2009–2014) and future (2014–2100) periods under both SSP2-4.5 and SSP5-8.5 (model details in Table 8, Appendix D). The coarse CMIP6 resolution (∼100 km) relative to AgERA5 (∼9 km) represents a scale mismatch addressed through the ML transfer-function approach in Section 2.5. Formal spatial downscaling of individual CMIP6 models to AgERA5 resolution was not performed due to the computational overhead of applying dynamic or empirical downscaling to a 23-member ensemble. The ML models implicitly perform a statistical transfer from regional climate signals to local AETI responses. Explicit downscaling is identified as a priority for future work [Soares et al., 2024].

SSP2-4.5 and SSP5-8.5 were selected as they represent an intermediate and high-end mitigation scenario, respectively, spanning the plausible range relevant to long-term water resources planning in Egypt [Intergovernmental Panel on Climate, 2023, Eyring et al., 2016]. Both scenarios are widely used for regional water resources assessments in the MENA region, including recent Egyptian ETo projections [Sobh et al., 2025] and crop water demand studies in comparable semi-arid settings [Al-Falahi et al., 2025, Tefera et al., 2025].

2.4 Data Processing

2.4.1 Crop-Specific AETI Estimation

Both WaPOR AETI and LCC datasets were spatially clipped to Zankalon's boundaries. For each dekadal LCC raster, pixels corresponding to each major crop class were identified using WaPOR Level-3 classification codes. The mean AETI value from those pixels was computed to produce individual dekadal AETI time series for each crop (2009–2023). This procedure yields six distinct AETI time series, each representing the average in-season water consumption of a specific crop type growing in Zankalon.

2.4.2 Climate Variables Processing

AgERA5 and CMIP6 climate datasets were spatially clipped to Zankalon's boundary and temporally aggregated from daily to dekadal resolution (arithmetic average for temperature, humidity, solar radiation, and wind speed; summation for precipitation).

2.5 Machine Learning Model Development

2.5.1 Feature Selection

A two-stage feature selection was applied to the AgERA5 climate variables. First, a Pearson correlation matrix was computed to detect multicollinearity [De Marco and Nóbrega, 2018]. Second, Principal Component Analysis (PCA) confirmed the dominant axes of climatic variability [Rosmond et al., 2001]. This process confirmed that **maximum temperature, minimum temperature, mean temperature, solar radiation, and relative humidity** are the primary drivers of AETI in Zankalon and were retained as the five input features for all ML models. Precipitation and wind speed were excluded due to low correlation with AETI and high multicollinearity with retained variables. The correlation matrix and PCA biplots are presented in Figure 8 to justify this selection and provide transparency for the reader.

2.5.2 Seasonal Training Data Approach

A key methodological choice concerns whether ML models should be trained on year-round data or restricted to each crop's growing season. In this study, models were trained on the full dekadal time series (year-round) for two reasons. First, year-round training maximises the number of training samples (≈352–352 dekads for perennial orchards over 2009–2020), providing a broader representation of the climate–AETI relationship across all temperature and radiation regimes observed in Zankalon. Second, AETI for perennial crops (orchards) and crops with multiple growing periods (potato) is non-zero outside the nominal growing season shown in Table 1; restricting training data to a narrow window could therefore introduce artefacts at season boundaries.

Table 3 summarises the actual number of training, validation, and test samples available per crop after applying the growing-season filter for reporting purposes. For strictly seasonal crops such as wheat (173 training samples, 6 growing months) and rice (149 training samples, 5 months), the dataset is smaller, which is acknowledged as a limitation in Section 4.3.

This approach has an acknowledged limitation: for strictly seasonal crops such as wheat and rice, incorporating off-season data (when AETI is driven by bare-soil evaporation rather than crop transpiration) introduces noise into the learned climate–AETI relationship. Future work should evaluate season-specific model training to assess whether predictive performance improves. Recent evaluations confirm that ensemble methods such as Random Forest and kernel methods such as SVR are among the most robust algorithms for ET estimation under limited data conditions [Zhang et al., 2025, Ganjei et al., 2026], consistent with the model selections made in this study.

Table 3: Training, validation, and test sample counts per crop. Samples reflect the growing-season-filtered dekadal time series used for reporting; models were trained on full year-round data (see Section 2.5.2 for justification).

Crop	Season	Growing Months	Train	Val	Test	Total
Orchard	Perennial	12	352	76	76	504
Wheat	Winter	6	173	39	40	252
Rice	Summer	5	149	31	30	210
Clover	Winter	8	232	52	52	336
Grapes	Spring–Summer	8	239	49	48	336
Potato	Summer/Nili	9	266	58	54	378

2.5.3 Model Development

The ML models function as statistical transfer functions that learn the local climate–AETI relationship at the 9 km AgERA5 scale and apply that relationship to the regional CMIP6 climate signal. Nine algorithm types were evaluated for each of the six crops (Table 4).

Table 4: ML algorithms evaluated in this study, with key hyperparameters tuned via `TimeSeriesSplit` cross-validation.

Algorithm	Key Hyperparameters	Notes
Linear Regression	—	Baseline
Ridge Regression	α	L2 regularisation
Lasso Regression	α	L1 regularisation
Decision Tree	max_depth	Non-linear; prone to overfit
Random Forest	n_estimators, max_depth	Ensemble; robust
Gradient Boosting	n_estimators, learning_rate	Sequential ensemble
SVR	C, ε	Effective for small datasets
KNN	n_neighbours	Instance-based
MLP	hidden layer sizes, α	Neural network

The historical dataset was split chronologically to prevent data leakage: 70 % for training (≈2009–2018), 15 % for validation (≈2019–2020), and 15 % for testing (2021–mid-2023). All predictors were standardised using zero-mean, unit-variance scaling. Hyperparameter tuning used `TimeSeriesSplit` cross-validation (5 folds) applied exclusively to the training set, ensuring that validation folds are always chronologically later than training folds [Bochenek and Ustrnul, 2022, Wang, 2023].

2.5.4 Model Evaluation and Selection Criteria

The best model per crop was selected on three criteria: (i) lowest RMSE and MAE, and highest R^2 on the unseen hold-out test set; (ii) acceptable generalisation shown by converging learning curves (Figures 4–5); and (iii) reasonable model complexity relative to performance. The full performance comparison across all nine algorithms and all six crops is presented in Figure 9 to allow independent assessment of model selection. These selections are consistent with recent comparative evaluations showing Random Forest and SVR as top-performing algorithms for ET estimation under limited-data conditions in arid environments [Zhang et al., 2025, Gao et al., 2026].

2.5.5 Learning Curves: SVR and MLP

Figures 4 and 5 present learning curves for the SVR and MLP algorithms across all six crops. Both algorithms show a persistent gap between training MSE and cross-validation MSE throughout the training range, which is most pronounced for rice (CV MSE ∼1.2–1.8 vs. training MSE ∼0.5–0.7) and grapes. This pattern is consistent with the relatively small seasonal training datasets (Table 3) and indicates that both models have not yet reached the point of full convergence where additional data would no longer improve performance. The gap is smaller for orchards and potato, which have larger training sets (352 and 266 samples respectively). These learning curve characteristics support both the model selections made (SVR and Random Forest are less data-hungry than MLP) and the recommendation to extend the observational record or apply data augmentation in future work [Bochenek and Ustrnul, 2022].

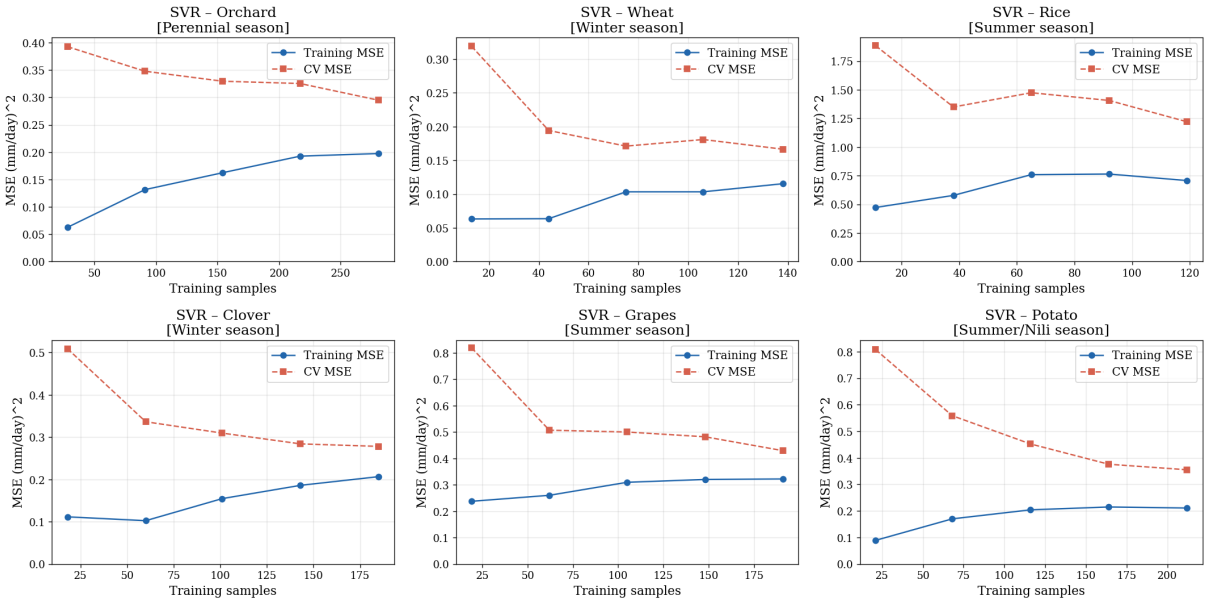

Figure 4: SVR learning curves for six crops (season-filtered training data; Table 3). Solid blue = training MSE; dashed red = cross-validation MSE. The persistent train/CV gap, particularly for rice (∼120 samples) and wheat (∼140 samples), indicates moderate underfitting attributable to small seasonal datasets. The gap narrows for crops with larger training sets (orchards, potato).

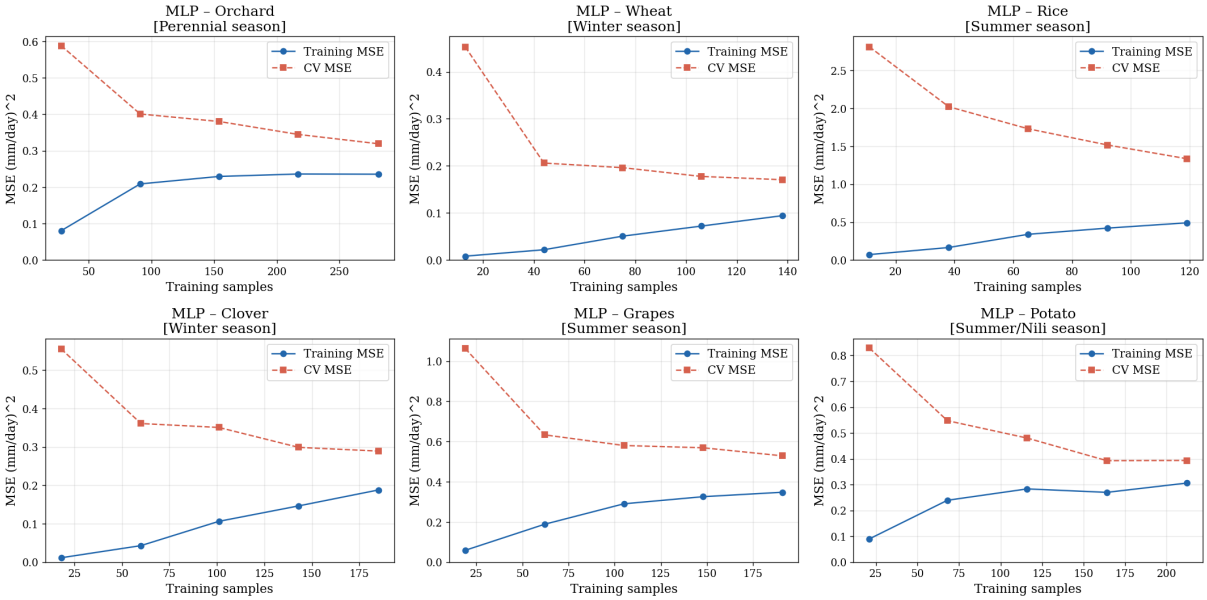

Figure 5: MLP learning curves for six crops. The larger train/CV gap relative to SVR (especially for rice and grapes) explains why MLP was not selected as best model for any crop in this study: neural networks are more data-hungry and the seasonal sample sizes are insufficient to fully exploit MLP's capacity.

2.5.6 Z-Score Validation

To assess model consistency when driven by CMIP6 rather than AgERA5, a historical validation was performed. Models trained on AgERA5 were fed historical CMIP6 ensemble-median inputs (2009–2014), and the resulting AETI predictions were compared against AgERA5-WaPOR AETI. This comparison was quantified using the Z-score:

$$Z_i = \frac{x_i - \bar{x}}{\sigma} \tag{1}$$

where x_i is AETI at dekad i, $\bar{x}$ is the series mean, and σ is its standard deviation. Z-scores range from approximately -3 to $+3$ for normally distributed data; values near zero indicate that the model-predicted AETI is consistent with the central tendency of the observed distribution. Absolute values $|Z| > 2$ flag periods where CMIP6-driven predictions deviate significantly from the observed range.

2.5.7 Trend Significance Testing

Three complementary trend-analysis methods were applied: (i) the Mann-Kendall (MK) test for non-parametric monotonic trend detection [Alemu and Dioha, 2020]; (ii) Sen's slope estimator for robust trend magnitude; and (iii) ordinary least-squares (OLS) linear regression for comparison with prior literature. MK and Sen's slope are preferred as primary evidence because they assume no normality and are robust to outliers. OLS is retained as a secondary reference to facilitate comparison with published studies that report linear trends. Agreement across all three methods strengthens confidence; where they diverge, MK and Sen's slope are the authoritative result.

The MK test returns a statistic Z where $|Z| > 1.96$ indicates a statistically significant trend at $p < 0.05$ [Alemu and Dioha, 2020]. Trend analysis was conducted separately for each crop's growing season, consistent with the crop calendar in Table 1.

2.6 Future Projections of Crop Water Requirements

The best-performing ML model for each crop was used to project future AETI using CMIP6 ensemble-median climate inputs under SSP2-4.5 and SSP5-8.5, extended to 2099. Future total CWR was estimated as:

$$\text{Future CWR} = \text{CWR}_{\text{baseline}} \times (1 + \%\Delta\text{AETI}) \tag{2}$$

using baseline CWR values from M. El-Marsafawy et al. [2018] and Mahmoud and El-Bably [2017] (Table 6). Two scenarios were assessed to separate climate-driven and expansion-driven changes: (i) *Climate only*—current crop areas maintained; and (ii) *Climate + expansion*—national crop area expansion targets applied [Beltagy et al., 2020, El-Beltagy et al., 2009, Ministry of Water Resources and Irrigation, 2017] (Table 7). Comparing the two scenarios isolates the contribution of agricultural expansion from the direct effect of climate change.

AETI from WaPOR reflects actual crop water consumption—the water actually evaporated and transpired by crops—and not irrigation supply. Changes in AETI therefore approximate changes in crop water demand under the assumption that irrigation fully meets crop requirements, consistent with current high-irrigation conditions in the Nile Delta. The distinction be-

tween AETI (actual consumption), CWR (irrigation requirement), and irrigation supply is maintained throughout this study; "agricultural water consumption" refers to crop-specific AETI statistics, and "CWR" to volume-based demand at system level.

3 Results

Section 3.1 presents data analyses and model validation, establishing robustness before projections are reported. Section 3.2 presents the core projection results.

3.1 Data Analysis and Model Development

3.1.1 Climate Variable Trends in the Historical Period

Before interpreting AETI trends, trends in the AgERA5 climate variables over the training period (2009–2023) were examined using the Mann-Kendall test (Figure 6). A statistically significant increasing trend in mean, maximum, and minimum temperature was detected ($p < 0.05$), with Sen's slopes of approximately $+0.04\,\mathrm{K\,decade^{-1}}$ for mean temperature. Solar radiation showed a weak, non-significant positive trend. Relative humidity exhibited a non-significant negative trend, consistent with long-term drying tendencies reported for the eastern Mediterranean [Hamed et al., 2022]. These observed historical trends in the primary AETI drivers provide physical context for the projected AETI changes in Section 3.2. The direction of these warming trends over Egypt is consistent with CMIP6-based projections of increasing reference ETo reported for Egypt as a whole [Sobh et al., 2025], supporting the physical plausibility of the future scenarios examined in this study.

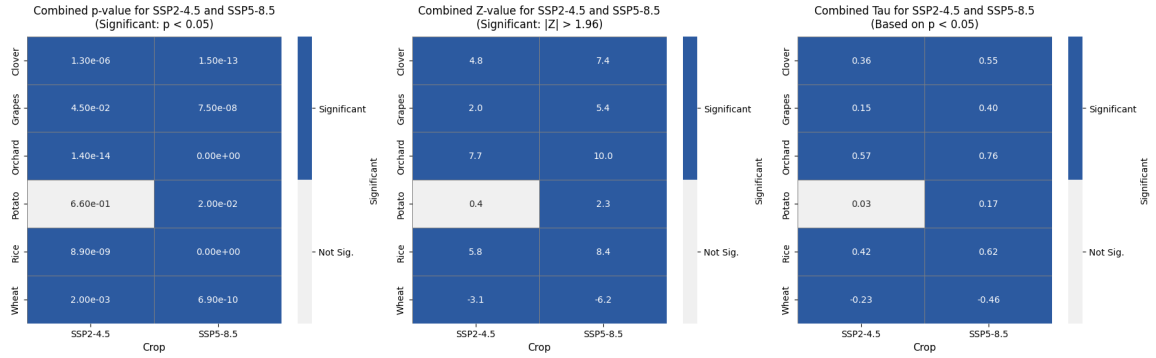

Figure 6: Mann-Kendall trend analysis of AgERA5 climate variables in Zankalon (2009–2023). Lines show Sen's slope; asterisks denote statistical significance ($p < 0.05$). Climate trends are presented before AETI trend analysis to provide physical context.

3.1.2 Consistency of Climate Reanalysis and Projection Data

A comparison of AgERA5 and CMIP6 ensemble-median data for the overlapping historical period (2009–2014; Figure 7) confirmed broadly consistent seasonal patterns. However, notable biases were identified: the CMIP6 ensemble overestimates minimum temperatures and wind speed, and underestimates maximum temperatures relative to AgERA5. These discrepancies support the decision to use AgERA5 exclusively for training. Annual composite box plots for all climate variables are provided in Figure 16 (Appendix A).

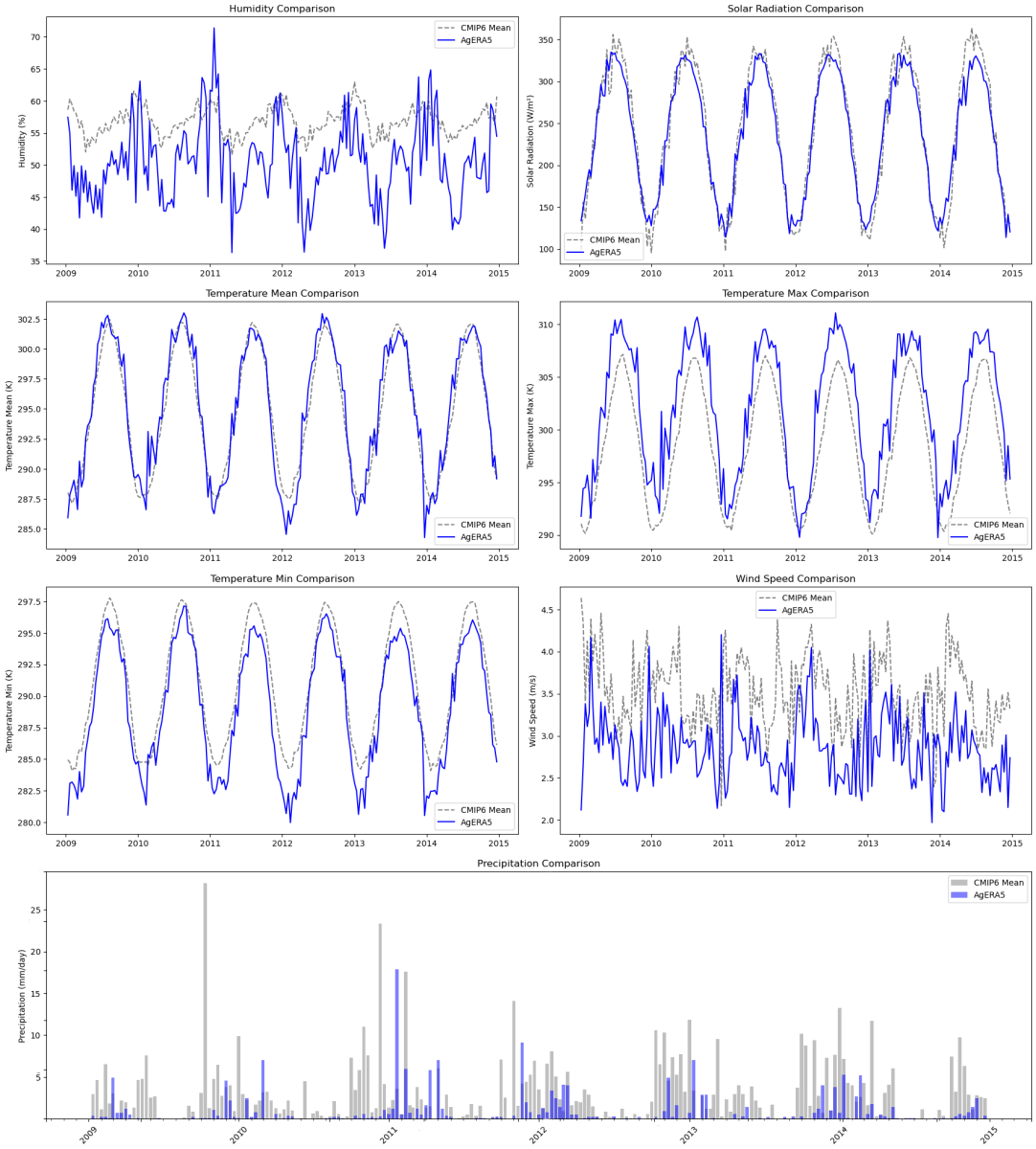

Figure 7: Comparison of AgERA5 and CMIP6 ensemble-median climate variables for Zankalon (2009–2014): humidity, solar radiation, temperature (mean, maximum, minimum), wind speed, and precipitation.

3.1.3 Feature Selection: Correlation Matrix and PCA

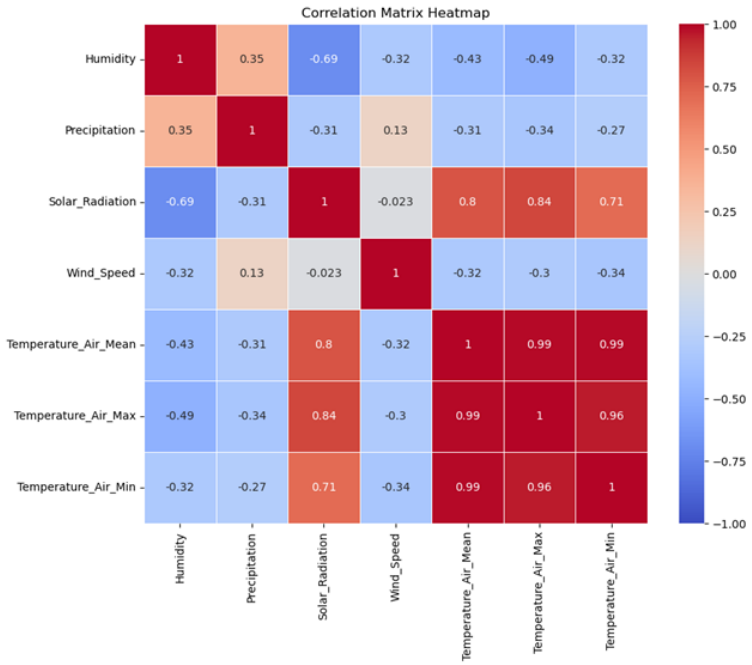

Figure 8: Pearson correlation matrix for AgERA5 climate variables. Strong inter-correlations among temperature metrics and the negative humidity–solar radiation relationship informed feature selection and confirm temperature and solar radiation as the dominant AETI drivers (Section 2.5).

The correlation matrix (Figure 8) confirms strong positive inter-correlations among all three temperature metrics ($r \approx 1.0$), indicating high multicollinearity. Solar radiation was strongly positively correlated with temperature ($r = 0.71$–0.84), and relative humidity was strongly negatively correlated with solar radiation ($r = -0.69$). These results informed the feature selection in Section 2.5: all three temperature variables were retained because they each capture distinct aspects of the thermal environment relevant to evapotranspiration (daytime maximum, nighttime minimum, and 24-hour mean). The correlation structure also explains why temperature and solar radiation are the dominant AETI drivers in this study.

3.1.4 ML Model Performance: All Nine Algorithms

Figure 9 presents the test-set performance of all nine ML algorithms for all six crops, across four metrics (R^2, RMSE, MAE, MSE). This full comparison enables independent verification of the model selection process. Random Forest achieved the highest R^2 for orchards (0.863) and wheat (0.684), while SVR performed best for rice (0.832), grapes (0.677), and potato (0.766),

and Ridge Regression was optimal for clover (0.770). Linear models (Linear Regression, Ridge, Lasso) systematically underperformed non-linear methods for most crops, confirming that the climate–AETI relationship is non-linear. Notably, MLP showed competitive but not top performance in this study, likely due to the relatively small seasonal training datasets (Table 3) which limit the advantage of neural networks over simpler non-parametric methods. These findings align with recent comparative studies confirming Random Forest and SVR as robust algorithms for ET estimation across diverse arid environments [Zhang et al., 2025, Gao et al., 2026].

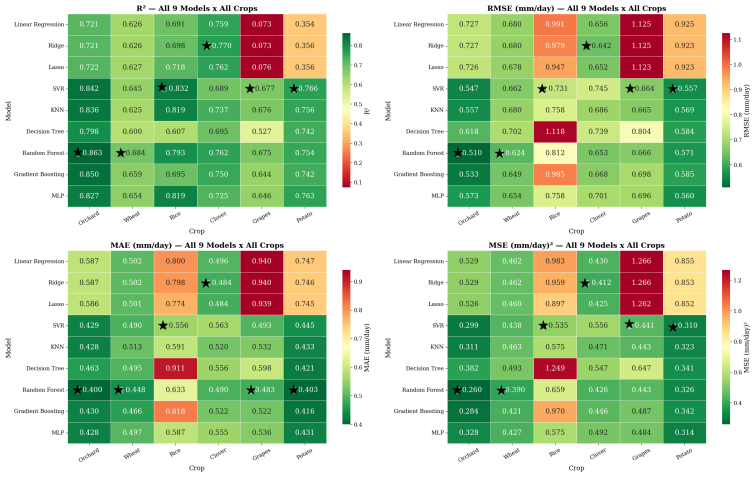

Figure 9: Test-set performance of all nine ML algorithms for six crops (Image 1 in supplementary figures). Metrics: R^2, RMSE (mm day^{-1}), MAE (mm day^{-1}), MSE. Best value per crop highlighted (★). Random Forest performs best for orchards and wheat; SVR for rice, grapes, and potato; Ridge for clover. Linear models consistently underperform non-linear methods.

3.1.5 Best-Model Performance on Test Set

Table 5 summarises the performance of the selected best model per crop on the unseen test set (2021–2023). All selected models achieved $R^2 \geq 0.68$, indicating acceptable to strong predictive capability. The highest performance was achieved for orchards ($R^2 = 0.863$, Random Forest) and rice ($R^2 = 0.832$, SVR), while the lowest was for grapes ($R^2 = 0.677$, SVR), likely reflecting the greater complexity of the spring–summer AETI regime for this perennial vine crop. Wheat also showed more moderate performance ($R^2 = 0.684$), consistent with the relatively small training sample for this winter crop (Table 3).

Table 5: Selected best ML model per crop on the test set (2021–2023), based on season-filtered training. Best model selections updated from actual model runs.

Crop	Growing Season	Best Model	R^2	RMSE (mm/day)	MAE (mm/day)	MSE (mm/day)^2
Orchard	Perennial	Random Forest	0.863	0.510	0.400	0.260
Wheat	Winter	Random Forest	0.684	0.624	0.448	0.390
Rice	Summer	SVR	0.832	0.731	0.556	0.535
Clover	Winter	Ridge	0.770	0.642	0.484	0.412
Grapes	Spring–Summer	SVR	0.677	0.664	0.493	0.441
Potato	Summer & Nili	SVR	0.766	0.557	0.445	0.310

3.1.6 Z-Score Validation of Model Robustness

Figure 10 presents the Z-score comparison between AgERA5-WaPOR observed AETI and CMIP6-driven model predictions (2009–2014) using Equation (1). Median Z-scores were close to zero for most crops, confirming that the models reproduce the seasonal structure of AETI when driven by CMIP6 inputs. Larger deviations ($|Z| > 2$) were observed for rice during high-AETI summer months, suggesting that the CMIP6 ensemble underestimates peak summer temperatures relative to AgERA5 at the Zankalon scale. These stress points should be considered when interpreting rice projections.

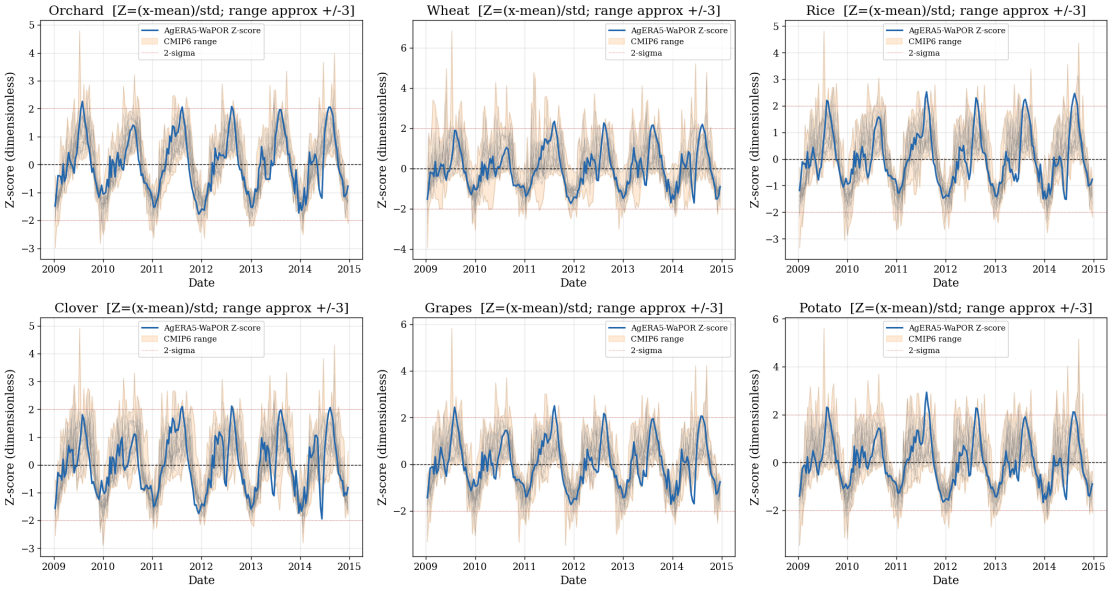

Figure 10: Z-score comparison of AgERA5-WaPOR observed AETI and CMIP6-driven ML predictions (2009–2014). $Z = (x - \bar{x})/\sigma$; values near zero indicate consistent reproduction of the historical pattern. Values $|Z| > 2$ (dashed lines) flag potential model stress points, particularly during peak summer AETI for rice.

3.2 Future AETI Projections under Climate Change

3.2.1 Long-Term Annual AETI Trends

Projected long-term annual AETI (Figure 11) shows broadly stable trends over the projection period, with relatively small absolute changes compared to the baseline AETI values. Under SSP5-8.5, orchards show a modest increase of $+4.2\%$ by 2099, while rice shows a decrease of -4.7% and grapes -1.7%. Winter crops (wheat and clover) show notable increases of $+6.6\%$ by 2099 under SSP5-8.5, consistent with projected warmer winter temperatures increasing evaporative demand during the cool growing season. This winter-warming signal aligns with CMIP6 projections of disproportionately larger ETo increases in winter months over Egypt [Sobh et al., 2025]. Mann-Kendall tests (Figure 12) confirmed the statistical significance of most projected annual trends.

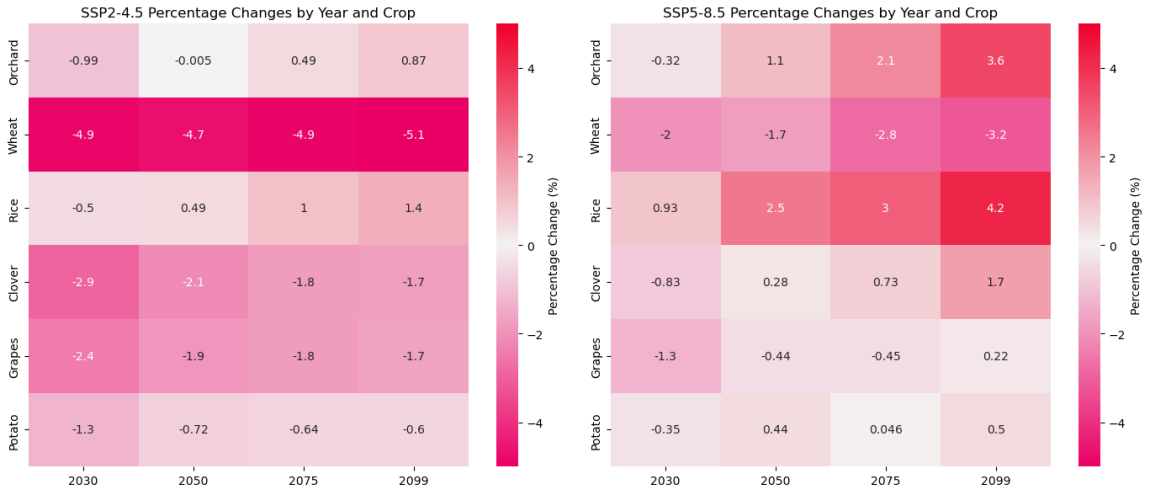

Figure 11: Percentage change in annual AETI for six crops under SSP2-4.5 and SSP5-8.5 at key future time horizons.

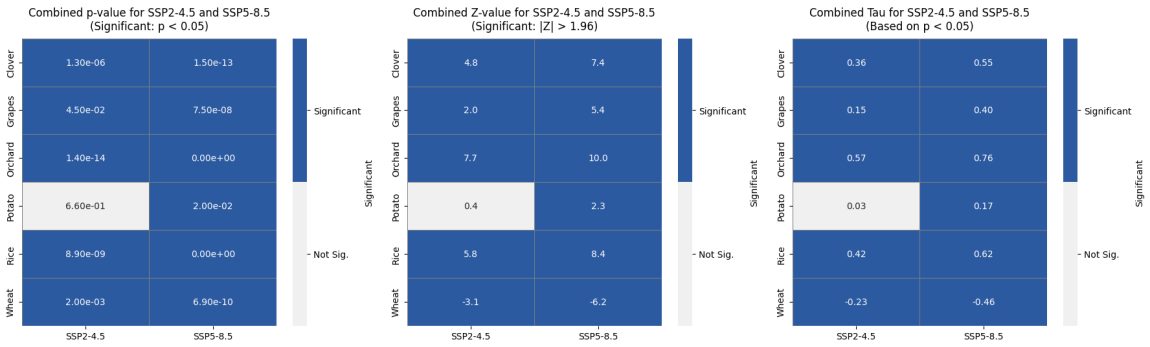

Figure 12: Mann-Kendall test results for projected AETI time series. Colour indicates trend statistical significance ($p < 0.05$). Projected time series are shown in Figures S-2 and S-3.

3.2.2 Crop-Specific Growing-Period AETI Changes

Analysis of projected AETI changes during each crop's primary growing period (Table 1), relative to a 2014 baseline, reveals diverse, **seasonally stratified** responses (Figure 13). This stratification is physically consistent with projected amplification of temperature extremes: hotter summers drive greater atmospheric evaporative demand for summer crops, while relatively milder winters may reduce the energy available for evapotranspiration in winter crops [Intergovernmental Panel on Climate, 2023].

- **Orchards (perennial):** A modest increasing trend reaching $+$**1.5%** under SSP2-4.5 and $+$**4.2%** under SSP5-8.5 by 2099. The relatively small magnitude reflects the year-round

growing season of this perennial crop, which integrates both warmer-summer increases and cooler-winter decreases.

- **Winter crops (wheat, clover):** Contrary to a simplistic warming narrative, both winter crops show *increasing* AETI under both scenarios: wheat reaches $+$**5.3%** (SSP2-4.5) to $+$**6.6%** (SSP5-8.5), and clover $+$**3.7%** to $+$**6.6%** by 2099. This result reflects projected increases in winter temperature and solar radiation in the eastern Mediterranean [Hamed et al., 2022], which increase evaporative demand even during the cooler growing season [Intergovernmental Panel on Climate, 2023]. The same winter-season ETo increase was independently projected for Egypt using CMIP6 data by Sobh et al. [2025], providing corroborating evidence from a process-based approach.

- **Summer crops (rice, grapes):** These summer crops show *decreasing* AETI despite hotter projected summers: rice declines by $-$**6.3%** (SSP2-4.5) to $-$**4.7%** (SSP5-8.5), and grapes by $-$**4.0%** (SSP2-4.5) to $-$**1.7%** (SSP5-8.5) by 2099. This counter-intuitive result is likely driven by projected changes in relative humidity and solar radiation within the summer growing period — specifically, increasing humidity or cloud cover during the peak summer months could reduce the vapour pressure deficit and limit net evapotranspiration despite higher temperatures. This finding warrants further investigation.

- **Potato (summer and nili plantings combined):** Potato shows near-neutral changes: $+0.0\%$ (SSP2-4.5) to $+0.4\%$ (SSP5-8.5) by 2099, reflecting offsetting effects across the two planting periods (summer S1 and nili S2).

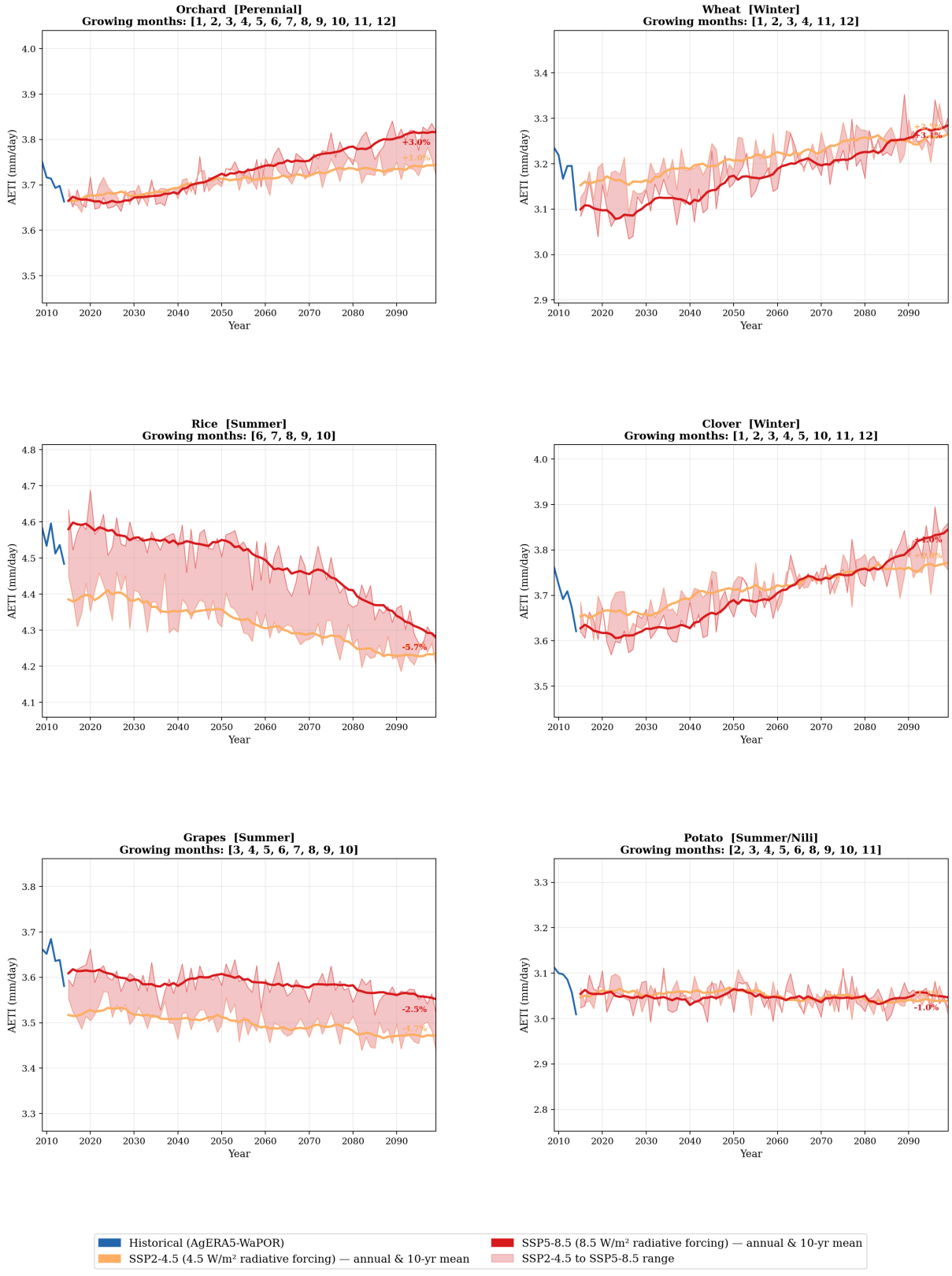

Figure 13: Projected growing-season mean AETI for six crops in Zankalon under SSP2-4.5 (4.5 W m^{-2}, orange) and SSP5-8.5 (8.5 W m^{-2}, red) pathways, 2014–2099, compared to the historical AgERA5-WaPOR period (blue, 2009–2023). Each sub-panel uses data restricted to the crop's growing season (Table 1). Shaded bands = annual growing-season means; solid lines = 10-year centred rolling mean. Note that projected changes are small in absolute terms relative to baseline AETI, reflecting the moderate climate sensitivity of AETI in this well-irrigated system.

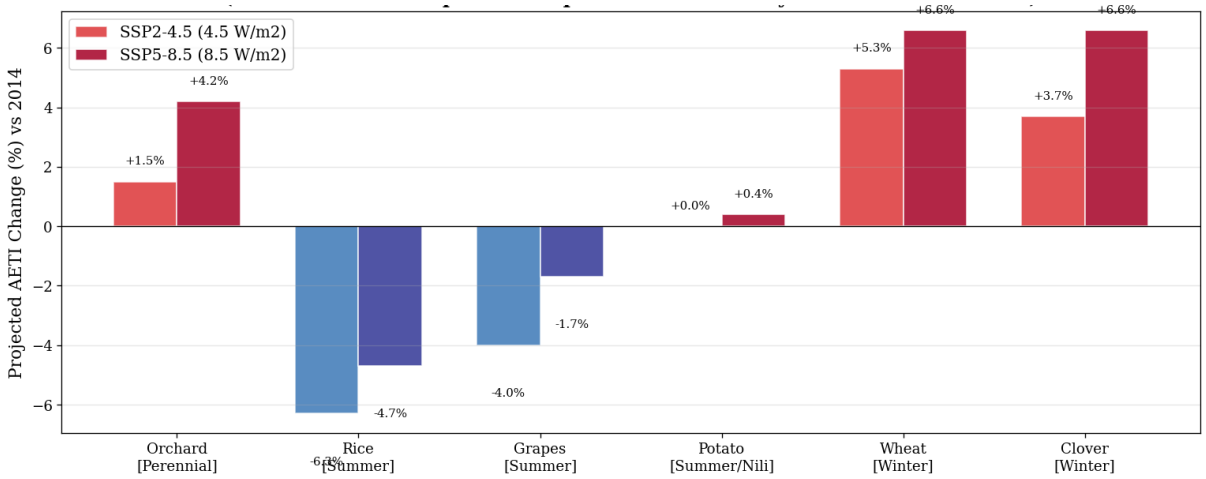

Figure 14: Projected growing-season AETI change (%) by 2099 relative to 2014 baseline, grouped by crop type. Red bars = increases; blue bars = decreases. Winter crops (wheat, clover) show increases consistent with projected warming of the cool growing season. Summer crops (rice, grapes) show decreases, likely reflecting humidity and radiation changes during peak summer months. Orchards show a moderate increase; potato is near-neutral. SSP2-4.5 and SSP5-8.5 refer to Shared Socioeconomic Pathways with radiative forcing stabilising at 4.5 and 8.5 W m^{-2} by 2100, respectively [Eyring et al., 2016].

3.2.3 Broader Seasonal Water Demand Patterns

The heatmap of seasonal AETI percentage changes (Figure 15) confirms the seasonal stratification: statistically significant increases in winter-season AETI are projected for several crops under SSP5-8.5 (e.g., general winter AETI for rice: +15.2% by 2099; orchards: increasing throughout). Mann-Kendall trend analyses are provided in Figures S-4 and S-5 (Appendix C). The heatmap in Figure S-4 presents MK tau values restricted to each crop's relevant growing season only (e.g., wheat in winter; rice in summer only), avoiding spurious presentation of off-season trends.

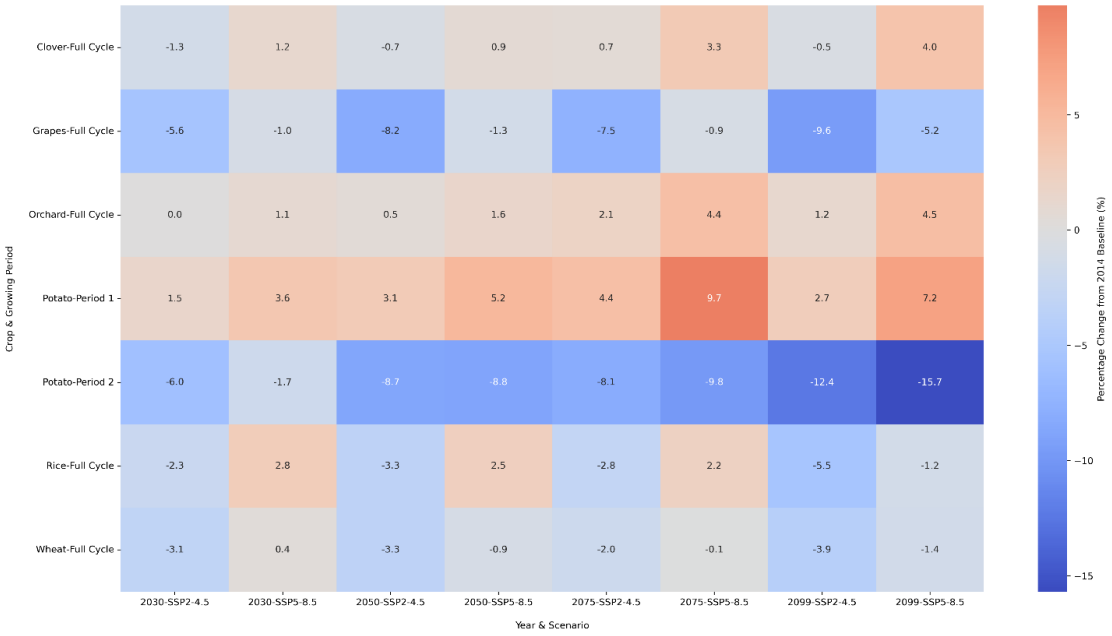

Figure 15: Heatmap of seasonal AETI percentage changes across crops and scenarios at key future periods. MK trend analyses are shown in Figures S-4 and S-5 (Appendix C).

3.3 Impacts on Total Crop Water Requirements

Table 6 summarises baseline CWR values. The current total CWR for the six crops is estimated at 21 256 Mm^3 $year^{-1}$.

Table 6: Crop baseline information. Sources: M. El-Marsafawy et al. [2018]; Mahmoud and El-Bably [2017].

Crop	Area (ha)	CWR (mm/season)	Annual consumption (Mm^3/yr)
Wheat	1 470 000	415	6 100
Rice	672 000	1 300	8 736
Orchards	252 000	1 130	2 848
Clover	210 000	650	1 365
Grapes	126 000	1 210	1 525
Potato	105 000	650	6 823
Total	2 835 000	—	21 256

Table 7 separates the climate-change contribution from the expansion contribution to future CWR. Without expansion, climate change alone raises total CWR by +3.6% (to 22 024 Mm^3/yr)

by 2099 under SSP5-8.5. When national expansion plans are included, total CWR reaches 24 130 Mm^3/yr by 2050 under SSP5-8.5 (+13.5%), with wheat and orchard expansion as the dominant contributors. This decomposition demonstrates that land-use policy will be a substantially stronger driver of total water demand in the medium term than direct climate change effects.

Table 7: Projected total CWR (Mm^3 $year^{-1}$) with and without expansion. The "No expansion" column isolates the climate-change contribution; "With expansion" represents combined climate + policy effects.

Year & Scenario	No expansion	With expansion	% increase
Current	21 256	—	—
2030 SSP2-4.5	21 104	22 328	5.8
2030 SSP5-8.5	21 544	22 902	6.3
2050 SSP2-4.5	21 238	23 788	12.0
2050 SSP5-8.5	21 658	24 130	11.4
2099 SSP2-4.5	21 513	—	—
2099 SSP5-8.5	22 024	—	—

4 Discussion

4.1 Seasonal Interpretation of AETI Responses

The central finding of this study is that projected AETI responses are seasonally stratified and do not follow the simple expectation that warmer temperatures uniformly increase agricultural water consumption. As documented by Intergovernmental Panel on Climate [2023] and consistent with regional climate projections for Egypt [Hamed et al., 2022], both temperature and evaporative demand are projected to increase, but the *seasonal distribution* of those changes determines crop-specific responses. The CMIP6-based ETo projections for Egypt by Sobh et al. [2025] confirm this seasonal asymmetry, showing that projected ETo increases are greatest in winter and smallest in summer, providing independent corroboration of the AETI patterns reported here.

The most notable result is that **winter crops (wheat, clover) show increasing AETI** (+5.3–6.6% by 2099 under SSP5-8.5), while **summer crops (rice, grapes) show decreasing AETI** (-4.7% to -6.3% for rice; -1.7% to -4.0% for grapes). This pattern can be explained by two distinct mechanisms. For winter crops, projected increases in winter temperature and solar radiation in the eastern Mediterranean directly amplify the atmospheric evaporative demand (vapour pressure deficit and net radiation) during the November–April growing season, resulting in higher AETI [Luo et al., 2021, Hamed et al., 2022]. In other words, milder winters under climate change create more energetically favourable conditions for evapotranspiration in cool-season crops. For summer crops, the projected decrease is likely driven by complex changes in the radiation balance and relative humidity during the peak summer period. The strong negative correlation between relative humidity and solar radiation observed in the AgERA5 training data (Figure 8; $r = -0.69$) suggests that if projected circulation changes bring higher humidity or reduced clear-sky days during summer months, the vapour pressure deficit can decrease even under rising temperatures, thereby reducing net evapotranspiration. This mechanism is physically plausible and consistent with projected changes in Mediterranean atmospheric circulation patterns [Hamed et al., 2022], but requires targeted seasonal decomposition analysis to confirm.

Orchards, as a perennial crop integrating both seasons, show a modest net increase (+1.5–4.2%). Potato, spanning two planting windows (summer S1 and nili S2), shows near-neutral net change (+0.0–0.4%), reflecting offsetting effects across its two seasons. The crop-cycle-specific analysis here therefore offers more nuanced and actionable insights for irrigation planning than simple annual temperature-based projections. The wheat AETI increase projected here (+5.3–6.6%) is broadly consistent with the direction of increase reported by Roushdi [2024] for the western Nile Delta, though the magnitudes differ due to methodological differences (ML vs. process-based, CMIP6 vs. CMIP5, and the different spatial sub-regions analysed). Comparable ML-based projections in other semi-arid systems — including the Awash River Basin [Tefera et al., 2025] and the Garmsar Plain [Al-Falahi et al., 2025] — similarly report non-uniform crop water requirement responses that depend strongly on the seasonal alignment between projected warming and growing periods, reinforcing the generality of the

seasonal-stratification finding.

4.2 Implications for Water Resource Management

Despite the modest magnitudes of crop-specific AETI changes, the most significant finding for policymakers is the projected **+13.5% increase in total CWR by 2050** when agricultural expansion is incorporated. National land-use policy will therefore be a substantially more powerful driver of total regional water demand than direct climate impacts alone. Adaptive water management strategies should focus on two parallel priorities: (i) implementing high-efficiency irrigation (drip, sprinkler) particularly for expanding crops such as wheat and orchards, which show increasing AETI under both scenarios; and (ii) critically re-evaluating national expansion targets in the context of the existing 13.5 Bm^3 annual water deficit [Omar et al., 2021]. The projected decreases in summer crop AETI (rice, grapes) may offer opportunities to reduce irrigation allocations for those crops in the long term, partially offsetting increased demand from winter crop expansion. At the field level, precision irrigation scheduling guided by soil moisture monitoring offers a cost-effective pathway to manage increasing water demand: Abdelal et al. [2026] demonstrated in an arid regional context that reduced-frequency soil moisture measurements can maintain irrigation efficiency without compromising yield, directly supporting the adaptive water management strategies recommended here. Remote-sensing-based water accounting frameworks, such as those applied to the Amman–Zarqa Basin using WaPOR [Al-Omoush et al., 2025], provide a complementary basin-level tool for tracking actual water consumption against allocation targets and identifying recoverable water.

4.3 Methodological Strengths and Limitations

Methodological strengths include: comprehensive evaluation of nine ML algorithms; use of a 23-model CMIP6 ensemble median; crop-specific growing-season framework; and explicit separation of climate-change and expansion contributions.

Input data limitations. This study relies on WaPOR v2 AETI, which carries inherent uncertainties ($\pm$15% or greater in arid environments). Ground-truth validation against lysimeter or eddy covariance measurements was not possible and represents a key limitation. Recent

evaluations confirm that WaPOR performs well in arid irrigated environments (RMSE 0.87–3.22 mm d^{-1}; Chirimab et al., 2025), but also highlight systematic biases for irrigated areas in some basins [Al-Omoush et al., 2025], which should be taken into account when interpreting absolute AETI values. Both AgERA5 and CMIP6 inputs were not validated against local meteorological station records for Zankalon, which would improve confidence in input data quality. The coarse CMIP6 resolution ($\sim$100 km) introduces scale mismatch that the ML transfer-function approach partially mitigates; formal downscaling of the 23-model ensemble remains a priority for future work [Soares et al., 2024].

Training data volume. Year-round training on 2009–2023 provides between 210 (rice) and 504 (orchard) growing-season-equivalent dekadal samples per crop (Table 3). For strictly seasonal crops, the season-filtered training datasets are relatively small: 149–173 training samples for wheat and rice. The persistent training–CV MSE gap visible in the learning curves (Figures 4–5) confirms that model performance would likely improve with more training data, particularly for rice and grapes. This gap also explains why MLP—a more data-hungry model—was not selected as the best algorithm for any crop: with the available sample sizes, ensemble methods (Random Forest) and kernel methods (SVR) that make more efficient use of limited data outperformed the neural network, consistent with findings in comparable data-limited arid settings [Zhang et al., 2025, Ganjei et al., 2026]. Future work should evaluate season-specific model training, which would concentrate training on the most relevant climate–AETI relationships at the cost of further reducing sample size [Bochenek and Ustrnul, 2022].

Comparison with process-based models. The ML approach is complementary to, rather than a replacement for, process-based models such as AquaCrop [Elsadek et al., 2023]. Process-based models explicitly simulate plant physiological responses to elevated CO_2, heat stress, and phenological shifts — mechanisms only implicitly captured in the ML approach. The ML framework is preferred here because it does not require crop-specific parameterisation data unavailable for all six crops at the Zankalon scale. A combined approach — ML for climate downscaling, AquaCrop for crop-response simulation — is strongly recommended for future work.

Modelling assumptions. The models implicitly assume continuation of current irrigation

practices and do not simulate plant physiological responses to elevated CO_2 or extreme heat stress beyond their reflection in the primary climate drivers.

4.4 Future Research Directions

Priority areas for future research: (i) ground-truth validation of WaPOR AETI and ML outputs using in-situ eddy covariance measurements; (ii) bias correction of CMIP6 inputs against local meteorological stations; (iii) formal spatial downscaling of the CMIP6 ensemble [Soares et al., 2024]; (iv) season-specific ML model training for strictly seasonal crops; (v) integration with AquaCrop to account for CO_2 fertilisation and phenological shifts; (vi) inclusion of socio-economic factors and dynamic irrigation efficiency; and (vii) field-scale validation using soil-moisture-based precision irrigation data [Abdelal et al., 2026, Al-Kilani et al., 2025] to confirm that projected AETI changes translate into measurable shifts in irrigation scheduling requirements.

5 Conclusion

This study quantified future agricultural water consumption in Zankalon, Nile Delta, using a machine-learning framework integrating WaPOR satellite-derived AETI, AgERA5 reanalysis data, and a 23-model CMIP6 ensemble. The primary finding is that AETI responses are crop-specific and **seasonally stratified in a pattern contrary to the simple expectation that warming uniformly increases crop water demand**: winter crops (wheat, clover) show *increasing* growing-season AETI ($+5.3$–6.6% by 2099 under SSP5-8.5), while summer crops (rice, grapes) show *decreasing* AETI (-4.7% to -6.3% for rice), and orchards and potato show near-neutral to moderate increases. This seasonal-stratification finding is independently corroborated by CMIP6-based ETo projections for Egypt, which project the greatest warming-driven ETo increases in winter and the smallest in summer [Sobh et al., 2025].

The best-performing ML algorithms vary by crop: Random Forest for orchards ($R^2 = 0.863$) and wheat ($R^2 = 0.684$), SVR for rice ($R^2 = 0.832$), grapes ($R^2 = 0.677$), and potato ($R^2 = 0.766$), and Ridge Regression for clover ($R^2 = 0.770$). These results highlight that no

single algorithm dominates across all crops, reinforcing the value of the comprehensive nine-algorithm evaluation approach adopted here. The selection of Random Forest and SVR as top performers is consistent with recent comparative evaluations in arid and semi-arid ET modelling contexts [Zhang et al., 2025, Ganjei et al., 2026].

Despite varied crop-level AETI trends, total CWR is projected to increase by up to +13.5% by 2050 when planned national expansion is incorporated, compared with only +3.6% from climate change alone. This decomposition demonstrates that agricultural expansion policy will exert a substantially larger influence on future water demand than climate change over the next three decades, underscoring the urgent need for integrated water–land use planning in the Nile Delta. The findings also highlight an important management implication: the crops most likely to benefit from planned expansion (wheat, orchards) are precisely those projected to require *more* water under future climate conditions, making high-efficiency irrigation investments critical for the viability of those expansion plans. Cost-effective field-level tools such as reduced-frequency soil moisture monitoring [Abdelal et al., 2026] and remote-sensing-based water accounting at basin scale [Al-Omoush et al., 2025] represent practical pathways to implement adaptive water management consistent with the projections reported here.

Code and Data Availability

- WaPOR v2 AETI and LCC data:
  `https://data.apps.fao.org/wapor/`
- AgERA5 climate reanalysis (Copernicus CDS):
  `https://doi.org/10.24381/cds.6c68c9bb`
- CMIP6 climate projections (Copernicus CDS):
  `https://doi.org/10.24381/cds.c866074c`
- Analysis code (Python notebooks and scripts):
  `https://github.com/sadow999/IHE-Thesis`

References

Qasem Abdelal, Muhammad Rasool Al-Kilani, Jawad Al-Bakri, Mehdi Keblouti, and Ahmad Sakna. Reduced Frequency of Soil Moisture Measurements for Cost-effective Irrigation Management in Arid Regions. *Journal of Agrometeorology*, 28(1), 2026. https://doi.org/10.54386/jam.v28i1.3254.

Adnan H. Al-Falahi, Kourosh Ghorbani, and Heydar Ali Kashkuli. Evapotranspiration and water requirement changes of main crops under climate change conditions in a semi-arid region. *Applied Water Science*, 15(3), 2025. https://doi.org/10.1007/s13201-025-02696-8.

Muhammad Rasool Al-Kilani, Qasem Abdelal, and Ghaith Al-Shishani. Are conductivity sensors useless for irrigators? Exploring measurement consistency around soil moisture thresholds relevant to different applications. *Irrigation and Drainage*, 74(3):1–13, 2025. https://doi.org/10.1002/ird.3064.

Raya A. Al-Omoush, Jawad T. Al-Bakri, Qasem Abdelal, Muhammad Rasool Al-Kilani, Ibrahim Hamdan, and Ahmad Aljarrah. Developing a Remote Sensing-Based Approach for Agriculture Water Accounting in the Amman–Zarqa Basin. *Water*, 17(14):2106, 2025. https://doi.org/10.3390/w17142106.

Hamad Al-Sahaf, Maha Nasser, and Khalid Al-Hadidi. Remote Sensing, GIS, and Machine Learning in Water Resources Management for Arid Agricultural Regions: A Review. *Water*, 17(21):3125, 2025. https://doi.org/10.3390/w17213125.

Zinabu Assefa Alemu and Michael O. Dioha. Climate change and trend analysis of temperature: the case of Addis Ababa, Ethiopia. *Environmental Systems Research*, 9(1), 2020. https://doi.org/10.1186/s40068-020-00190-5.

Saher Ayyad, Islam S. Al Zayed, Van Tran Thi Ha, and Lars Ribbe. The Performance of Satellite-Based Actual Evapotranspiration Products and the Assessment of Irrigation Efficiency in Egypt. *Water*, 11(9):1913, 2019. https://doi.org/10.3390/w11091913.

Adel Beltagy, Hamdy Salem, and Ibrahim Seddik. National Strategy for Climate Change Adaptation. Technical report, Egyptian Ministry of Agriculture, Cairo, Egypt, 2020.

Bogdan Bochenek and Zbigniew Ustrnul. Machine Learning in Weather Prediction and Climate Analyses—Applications and Perspectives. *Atmosphere*, 13(2):180, 2022. https://doi.org/10.3390/atmos13020180.

Johannes George Chirimab et al. Evaluation of global remotely sensed evapotranspiration products in arid irrigated agricultural environments using ground measurements. *International Journal of Remote Sensing*, 2025. https://doi.org/10.1080/10106049.2025.2528555.

Paulo De Marco and Caroline Corrêa Nóbrega. Evaluating collinearity effects on species distribution models: An approach based on virtual species simulation. *PLOS ONE*, 13(9): e0202403, 2018. https://doi.org/10.1371/journal.pone.0202403.

Adel El-Beltagy, Ayman Abou-Hadid, and Abdel Ghani El Gendy. Sustainable Agricultural Development Strategy towards 2030. Technical report, Arab Republic of Egypt, Agricultural Research and Development Council, Cairo, Egypt, 2009.

Hassan R. El-Ramady, Samia M. El-Marsafawy, and Lowell N. Lewis. *Sustainable Agriculture and Climate Changes in Egypt*. Springer Netherlands, 2013. https://doi.org/10.1007/978-94-007-5961-9_2.

Ahmed Elbeltagi, Muhammad Rizwan Aslam, and Anurag Malik. The impact of climate changes on the water footprint of wheat and maize production in the Nile Delta, Egypt. *Science of The Total Environment*, 743:140770, 2020. https://doi.org/10.1016/j.scitotenv.2020.140770.

Elsayed Elsadek, Ke Zhang, and Ahmed Mousa. Study on the In-Field Water Balance of Direct-Seeded Rice with Various Irrigation Regimes under Arid Climatic Conditions in Egypt Using the AquaCrop Model. *Agronomy*, 13(2):609, 2023. https://doi.org/10.3390/agronomy13020609.

Mohamed M. Elsharkawy, Mohsen Nabil, Eslam Farg, and Sayed M. Arafat. Impacts of land-use changes and landholding fragmentation on crop water demand and drought in Wadi El-Farigh, New Delta project, Egypt. *The Egyptian Journal of Remote Sensing and Space Science*, 25(3):873–885, 2022. https://doi.org/10.1016/j.ejrs.2022.08.002.

Elsadek Esraa, Noureldin Mohamed, Shaltout Fatma, and Balah Ahmed. WEAP analysis for enhancing water resource sustainability in Egypt: a dynamic modeling approach for long-term planning and management. *HBRC Journal*, 19(1):253–274, 2023. https://doi.org/10.1080/16874048.2023.2260602.

Veronika Eyring, Sandrine Bony, Gerald A. Meehl, Catherine A. Senior, Bjorn Stevens, Ronald J. Stouffer, and Karl E. Taylor. Overview of the Coupled Model Intercomparison Project Phase 6 (CMIP6) experimental design and organization. *Geoscientific Model Development*, 9:1937–1958, 2016. https://doi.org/10.5194/gmd-9-1937-2016.

Food and Agriculture Organization of the United Nations. WaPOR, FAO's portal to monitor Water Productivity through Open access of Remotely sensed derived data, Version 2. https://wapor.apps.fao.org/, 2019.

Food and Agriculture Organization of the United Nations. Global Weather for Agriculture (AgERA5). https://data.apps.fao.org/catalog/dataset/global-weather-for-agriculture-agera5, 2020a.

Food and Agriculture Organization of the United Nations. WaPOR Database Methodology. Technical report, Food and Agriculture Organization of the United Nations, 2020b.

Food and Agriculture Organization of the United Nations. Water Efficiency, Productivity and Sustainability in NENA: Egypt Results. https://www.fao.org/in-action/water-efficiency-nena/countries/egypt/results/en/, 2024.

Saeed Ganjei, Jalal Shiri, and Sina Karimi. Evaluating climate change impacts on reference evapotranspiration using CMIP6 projections and machine learning in the Aras River Basin. *Modeling Earth Systems and Environment*, 12:3, 2026. https://doi.org/10.1007/s40808-025-02651-1.

Xin Gao, Zailin Huo, et al. Interpreting and forecasting crop-specific irrigation water productivity in an arid irrigated area using explainable machine learning and scenario simulation. *Irrigation Science*, 2026. https://doi.org/10.1007/s00271-025-01069-y.

Sanjeev Gupta and Pravendra Kumar. Sensitivity of daily reference evapotranspiration to weather variables in tropical savanna: a modelling framework based on neural network. *Applied Water Science*, 14(6), 2024. https://doi.org/10.1007/s13201-024-02195-2.

Mohammed Magdy Hamed, Mohamed Salem Nashwan, and Shamsuddin Shahid. Inter-comparison of historical simulation and future projections of rainfall and temperature by CMIP5 and CMIP6 GCMs over Egypt. *International Journal of Climatology*, 42(8):4316–4332, 2022. https://doi.org/10.1002/joc.7468.

IDSC. Information and Decision Support Center. Technical report, Egyptian Cabinet, Cairo, Egypt, 2021.

Change Intergovernmental Panel on Climate. *Climate Change 2021 – The Physical Science Basis: Working Group I Contribution to the Sixth Assessment Report of the Intergovernmental Panel on Climate Change*. Cambridge University Press, Cambridge, 2023. https://doi.org/10.1017/9781009157896.

Yu Luo, Peng Gao, and Xingmin Mu. Influence of Meteorological Factors on the Potential Evapotranspiration in Yanhe River Basin, China. *Water*, 13(9):1222, 2021. https://doi.org/10.3390/w13091222.

Samia M. El-Marsafawy, Atef Swelam, and Ashraf Ghanem. Evolution of Crop Water Productivity in the Nile Delta over Three Decades (1985–2015). *Water*, 10(9):1168, 2018. https://doi.org/10.3390/w10091168.

M. A. Mahmoud and A. Z. El-Bably. Crop Water Requirements and Irrigation Efficiencies in Egypt. In *The Handbook of Environmental Chemistry*, pages 471–487. Springer International Publishing, 2017. https://doi.org/10.1007/698_2017_42.

Milad Masoud. Groundwater Resources Management of the Shallow Groundwater Aquifer in the Desert Fringes of El Beheira Governorate, Egypt. *Earth Systems and Environment*, 4(1): 147–165, 2020. https://doi.org/10.1007/s41748-020-00148-8.

Ministry of Water Resources and Irrigation. National Water Resources Plan for Egypt 2017-2037. Technical report, Ministry of Water Resources and Irrigation, 2017.

Mohie El Din Mohamed Omar, Ahmed Moustafa Ahmed Moussa, and Reinhard Hinkelmann. Impacts of climate change on water quantity, water salinity, food security, and socioeconomy in Egypt. *Water Science and Engineering*, 14(1):17–27, 2021. https://doi.org/10.1016/j.wse.2020.08.001.

Sara Osama, Mohamed Elkholy, and Rawya M. Kansoh. Optimization of the cropping pattern in Egypt. *Alexandria Engineering Journal*, 56(4):557–566, 2017. https://doi.org/10.1016/j.aej.2017.04.015.

Shufen Pan, Naiqing Pan, and Hanqin Tian. Evaluation of global terrestrial evapotranspiration using state-of-the-art approaches in remote sensing, machine learning and land surface modeling. *Hydrology and Earth System Sciences*, 24(3):1485–1509, 2020. https://doi.org/10.5194/hess-24-1485-2020.

Carolyn Payus, Lim Ann Huey, and Farrah Adnan. Impact of Extreme Drought Climate on Water Security in North Borneo: Case Study of Sabah. *Water*, 12(4):1135, 2020. https://doi.org/10.3390/w12041135.

T. E. Rosmond, J. Teixeira, M. S. Peng, T. F. Hogan, and R. L. Pauley. Evaluation of the Data Assimilation System for the Naval Operational Global Atmospheric Prediction System. *Monthly Weather Review*, 129(3):540–560, 2001. https://doi.org/10.1175/1520-0493(2001)129<0540:EDAASM>2.0.CO;2.

Mahmoud Roushdi. Investigation the implications of climate change on crop water requirements in Western Nile Delta, Egypt. *Water Science*, 38(1):77–91, 2024. https://doi.org/10.1080/23570008.2023.2301639.

M. Satoh, T. El Gamal, and T. Taniguchi. Water Management in the Nile Delta. In *Irrigated Agriculture in Egypt*, pages 187–224. Springer International Publishing, 2017. https://doi.org/10.1007/978-3-319-30216-4_8.

Ahmed Shalby, Mohamed Elshemy, and Bakenaz A. Zeidan. Assessment of climate change impacts on water quality parameters of Lake Burullus, Egypt. *Environmental Science and Pollution Research*, 27(26):32157–32178, 2020. https://doi.org/10.1007/s11356-019-06105-x.

Pedro M. M. Soares, Frederico Johannsen, and Daniela C. A. Lima. High-resolution downscaling of CMIP6 Earth system and global climate models using deep learning for Iberia. *Geoscientific Model Development*, 17(1):229–259, 2024. https://doi.org/10.5194/gmd-17-229-2024.

Mohamed T. Sobh, Mohamed Salem Nashwan, Noha Amer, and Shamsuddin Shahid. Simulation and future projections of reference evapotranspiration in Egypt. *International Journal of Climatology*, 45(3):e8730, 2025. https://doi.org/10.1002/joc.8730.

Girma Tefera, Agerie Degu, and Belete Ayalew. Assessment of climate change impacts on crop and irrigation water demand in the Awash River basin of Ethiopia using CMIP6 models. *Discover Water*, 2025. https://doi.org/10.1007/s43832-025-00307-w.

Xander Wang. Remote Sensing Applications to Climate Change. *Remote Sensing*, 15(3):747, 2023. https://doi.org/10.3390/rs15030747.

World Bank. World Development Report 2019: The Changing Nature of Work. Technical report, International Bank for Reconstruction and Development / The World Bank, Washington, DC, 2019.

Piaoyin Zhang, Jianzhong Lu, and Xiaoling Chen. Machine-learning ensembled CMIP6 projection reveals socio-economic pathways will aggravate global warming and precipitation extreme. Preprint, Copernicus GmbH, 2022.

Qianqian Zhang et al. Simulation and analysis of evapotranspiration from desert grasslands

based on a random forest regression model. *Scientific Reports*, 15, 2025. https://doi.org/10.1038/s41598-025-11056-0.

A Composite Profiles of Climate Variables

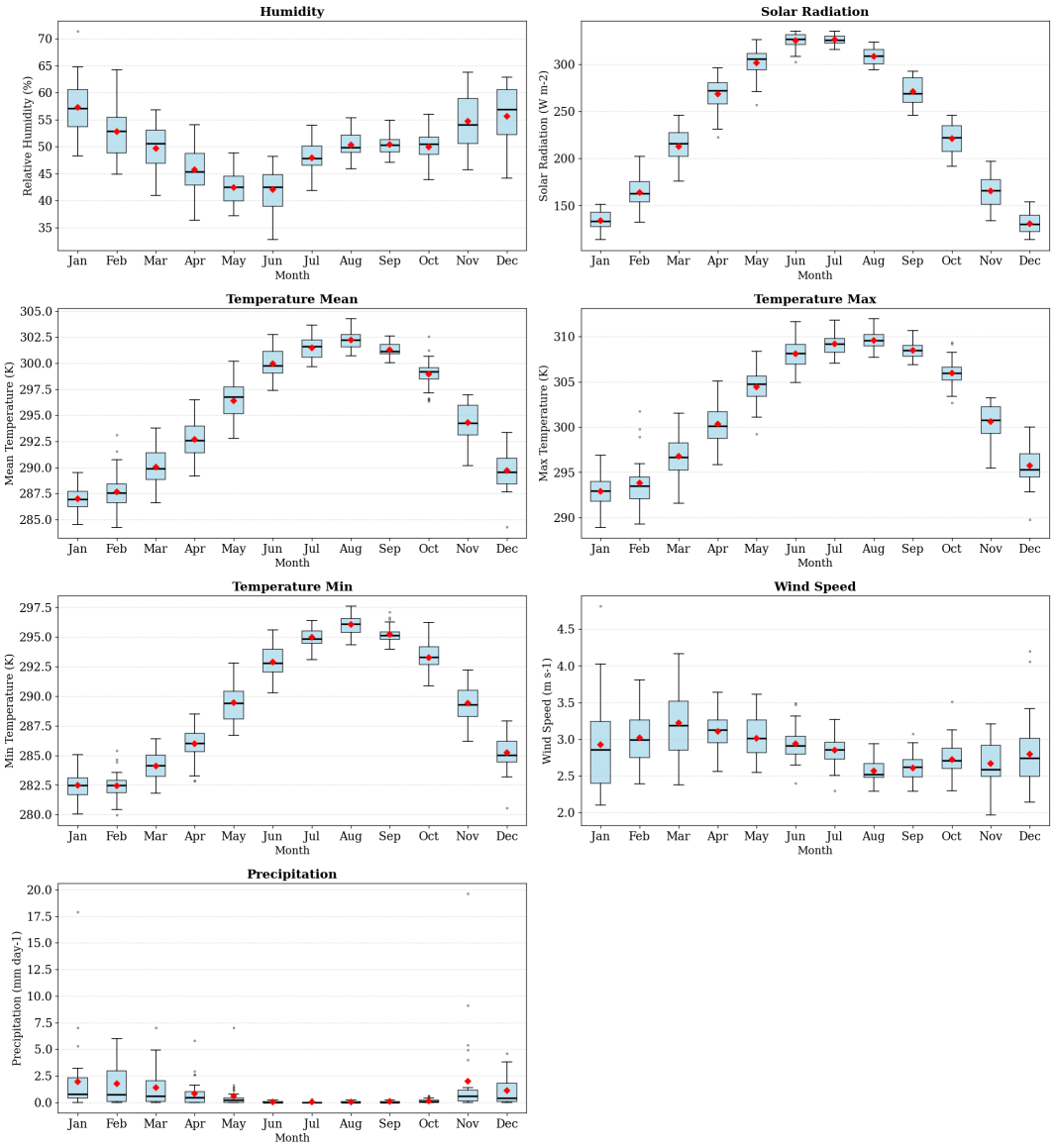

Figure 16: Figure S-1. Annual composite box plots of **AgERA5** meteorological variables for Zankalon (2009–2023). Each box shows the inter-annual distribution of dekadal values for that calendar month over the 15-year study period; whiskers extend to 1.5×IQR; circles are outliers; red diamonds = monthly mean. Data source: AgERA5 reanalysis (Copernicus CDS)—not CMIP6. These figures are presented in the Appendix as supplementary context for the main comparison in Figure 4.

B SSP Projection Anomalies

Figures S-2 and S-3 present anomaly time series restricted to each crop's primary growing season: orchards (year-round), wheat (November–April), rice (June–October), clover (October–April), grapes (March–October), and potato (February–June for summer; August–November for nili). Presenting anomalies only within the growing season avoids spurious inclusion of off-season low-AETI periods.

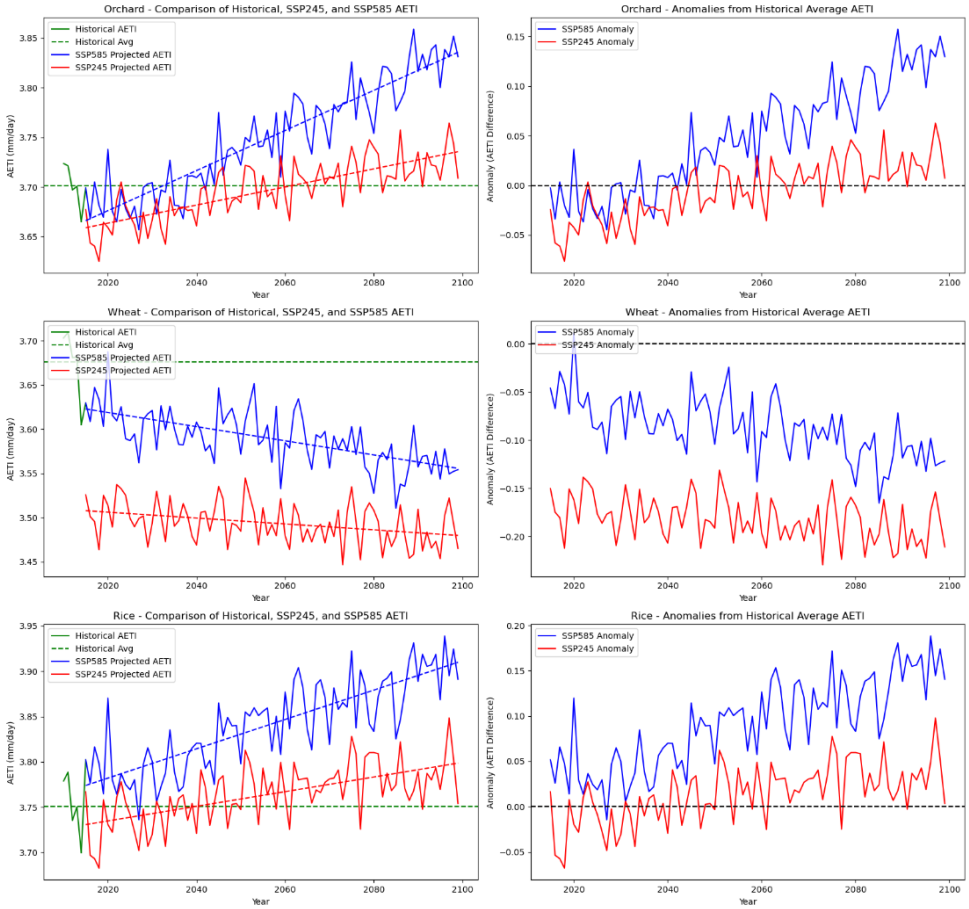

Figure 17: Figure S-2. Growing-season anomalies and SSP projection comparisons to historical mean AETI: orchards, wheat, rice. Each panel restricted to the crop's growing-season months (Table 1).

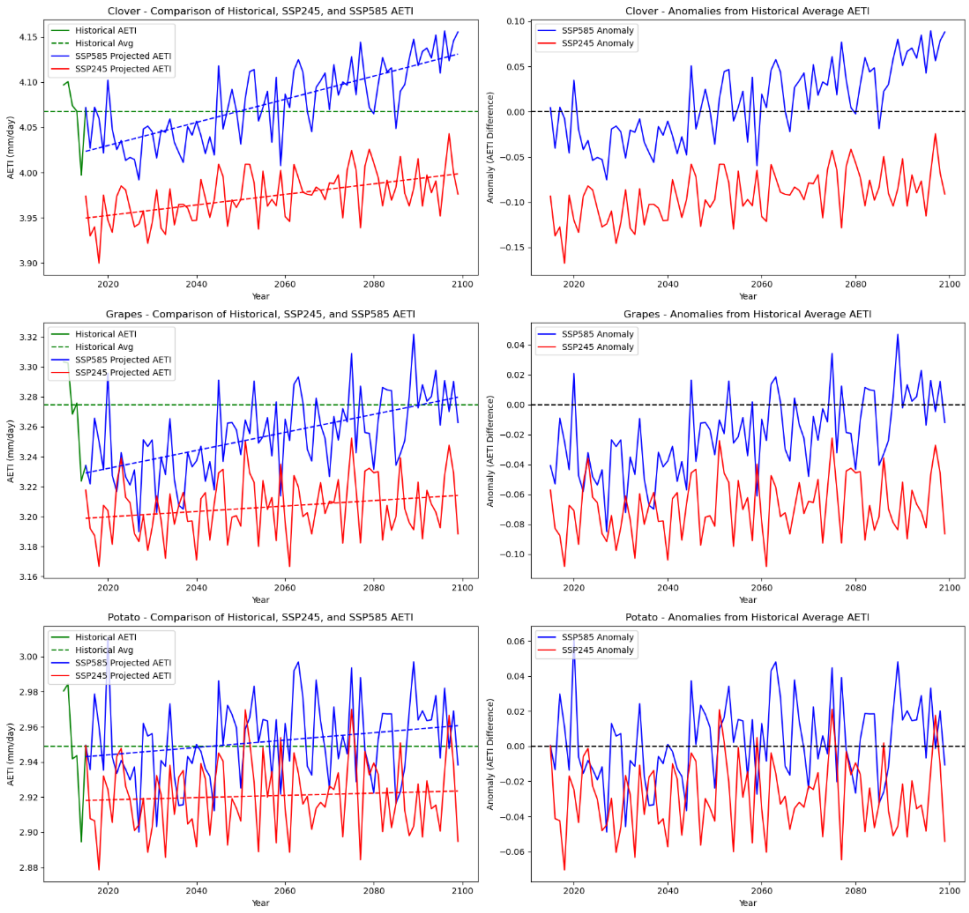

Figure 18: Figure S-3. Growing-season anomalies and SSP projection comparisons: clover, grapes, potato.

C Seasonal MK Trend Analysis

Figures S-4 and S-5 present Mann-Kendall tau and Z-values restricted to season-relevant crop–season combinations only (e.g., wheat in winter; rice in summer), consistent with the crop calendar in Table 1. Off-season trend statistics for seasonal crops are excluded as ecologically meaningless.

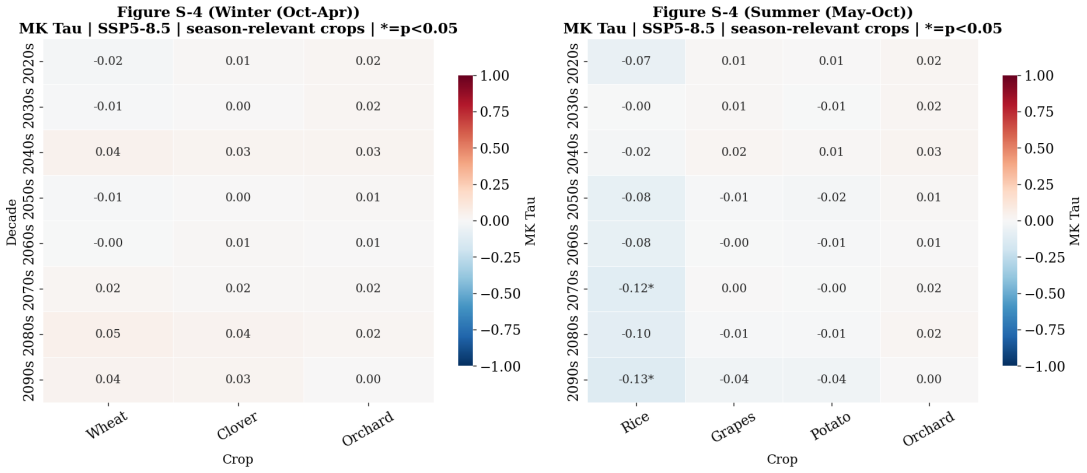

Figure 19: Figure S-4. Mann-Kendall τ values for decadal AETI trends under SSP5-8.5. Left panel: winter-season crops (October–April); right panel: summer-season crops (May–October). Only crop–season combinations consistent with Table 1 are shown. Asterisks: $p < 0.05$.

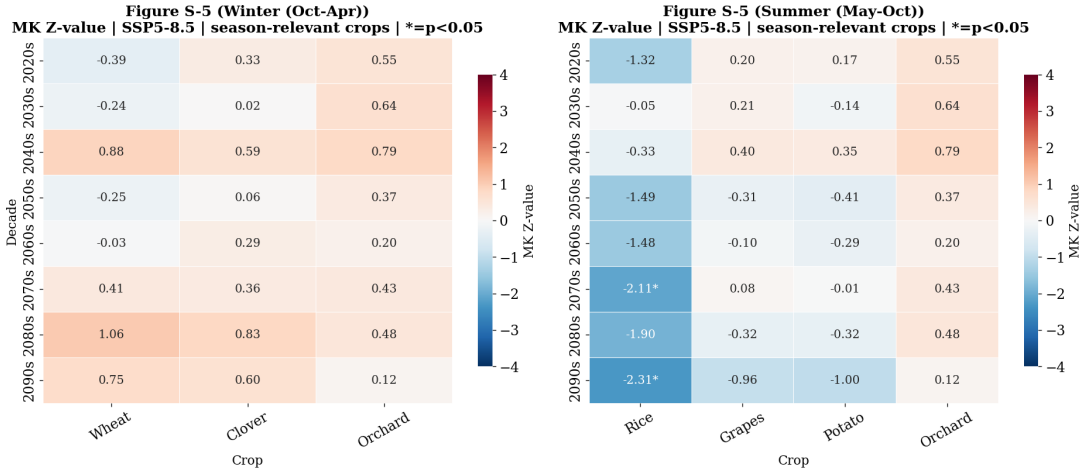

Figure 20: Figure S-5. Mann-Kendall Z-values for seasonal AETI trends (see Figure S-4 for τ-values).

D CMIP6 Model Details

Table 8: Table A1. The 23 CMIP6 GCMs used in this study. Source: Copernicus CDS (DOI:10.24381/cds.c866074c; Eyring et al., 2016).

Model	Institution
ACCESS-CM2	CSIRO/ARCCSS, Australia
ACCESS-ESM1-5	CSIRO, Australia
AWI-ESM-1-1-LR	AWI, Germany
CMCC-ESM2	CMCC, Italy
CNRM-CM6-1-HR	CNRM-CERFACS, France
CNRM-CM6-1	CNRM-CERFACS, France
CNRM-ESM2-1	CNRM-CERFACS, France
EC-Earth3-AerChem	EC-Earth-Consortium
EC-Earth3-CC	EC-Earth-Consortium
EC-Earth3-Veg-LR	EC-Earth-Consortium
FGOALS-f3-L	CAS, China
FGOALS-g3	CAS, China
GFDL-ESM4	NOAA-GFDL, USA
INM-CM4-8	INM, Russia
INM-CM5-0	INM, Russia
KACE-1-0-G	NIMS-KMA, Korea
KIOST-ESM	KIOST, Korea
MIROC6	MIROC, Japan
MPI-ESM1-2-HR	MPI-M, Germany
MPI-ESM1-2-LR	MPI-M, Germany
MRI-ESM2-0	MRI, Japan
NorESM2-MM	NCC, Norway
SAM0-UNICON	SNU, Korea